Spin-orbit effects in gas-phase chemical reactions

2 AUTHORS:

Paul J Dagdigian
Johns Hopkins University
323 PUBLICATIONS **6,108** CITATIONS

SEE PROFILE

Mark L. Campbell
United States Naval Academy
55 PUBLICATIONS **861** CITATIONS

SEE PROFILE

Chemical Reviews

Spin–Orbit Effects in Gas-Phase Chemical Reactions

PAUL J. DAGDIGIAN* and MARK L. CAMPBELL

Department of Chemistry, The Johns Hopkins University, Baltimore, Maryland 21218

Contents

I. Introduction

It has been appreciated for some time that different forms of reagent energy, e.g., translational, vibrational, rotational excitation, can have drastically different effects on the rate of a chemical reaction. The availability of state-specific rate constants can allow rather detailed inferences to be made on the dynamics of elementary-gas-phase reactions, with the aid of suitable theoretical input. Thus, considerable effort has been given to the measurement of detailed rate constants, or cross sections, with increasing levels of state resolution through experiments of greater sophistication. Today the field of molecular reaction dynamics is quite large, and there are several textbooks[1-3] and a number of comprehensive review articles[4-12] available.

In this review, we concentrate on experimental and theoretical investigations of spin–orbit effects in reactions involving atoms with both nonzero electronic angular momentum and spin multiplicity. We use the term spin–orbit effect to describe the differences in chemical reactivity of individual states of different total angular momentum J of an atomic multiplet. There has been growing interest in the study of reactions involving individual atomic fine-structure states since such investigations can reveal the importance of nonadiabatic effects in chemical reactions. Of special significance is the possibility of differences in reactivity between spin–orbit states whose differences in energy are small compared with the overall energetics of the reaction of interest. Branching fractions of spin–orbit states of product atoms are also of interest.

The importance of spin–orbit effects in chemical reactions would naively be expected to depend largely on the magnitude of the fine-structure splittings, particularly when the energy of the spin–orbit excitation is sufficient to overcome the reaction endoergicity. For reagent atoms in which the spin–orbit splittings are large, significant spin–orbit effects are anticipated due to the expected increase in reaction rate with total reactant energy. In fact, for heavy metals such as Sn-(^3P_J), Pb(^3P_J), and electronically excited Hg($^3P_J°$), in which the spin–orbit spacings are comparable to energy differences between different atomic electronic terms, large spin–orbit dependences on reaction rates have been observed, as we discuss in detail in section IV. By contrast, the different spin–orbit states of an atomic reagent with small fine-structure splitting might be expected to scramble completely as the atom approaches the reaction partner, leading to a negligible spin–orbit dependence. Nevertheless, a significant dependence of reactivity on spin–orbit states has been observed in a number of reactions of atoms with small fine–structure splittings, for example the metastable alkaline earth atoms and the lighter halogen atoms.

A convenient starting point for a theoretical understanding of spin-orbit effects involves consideration of the adiabatic potential energy surfaces correlating to the individual J states of an atomic multiplet. As first worked out in detail by Husain,[12] adiabatic correlation arguments in the strong spin–orbit coupling limit predict differing reactivities and product electronic state branching as a function of reagent spin–orbit state for many reactions. Several examples will be given later in this article. In many reactions, nonadiabatic mixing is very important, and dynamically based theoretical
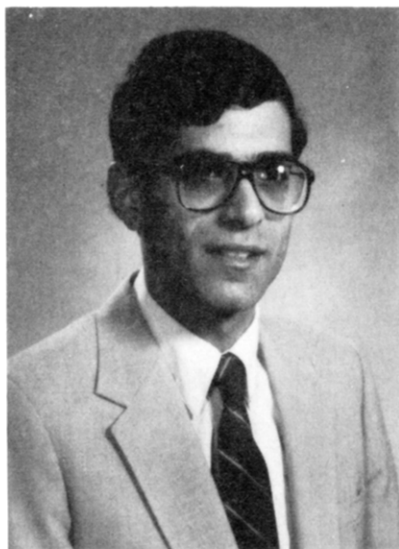
P. J. Dagdigian was born in Philadelphia, PA, in 1945. He obtained a B.A. degree from Haverford College in 1967 and a Ph.D. degree from the University of Chicago in 1972. After postdoctoral research at Columbia University, he joined the faculty of The Johns Hopkins University in 1974, where he is currently a professor of chemistry. He was an Alfred P. Sloan Fellow and a Camille and Henry Dreyfus Teacher–Scholar. Professor Dagdigian's research has principally involved the experimental investigation of the molecular dynamics of gas-phase collisional phenomena, including chemical reactions and nonreactive energy-transfer processes.
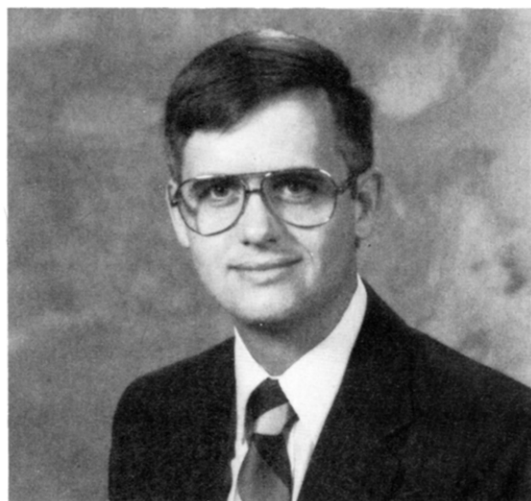
Mark L. Campbell was born in Salinas, CA, in 1956 and received degrees from Brigham Young University (B.S., *summa cum laude*, 1978, and M.S., 1980) and The Johns Hopkins University (M.A., 1985, Chemical Physics). After completing graduate school at Brigham Young in 1980, he accepted a commission in the U.S. Navy. He has held a faculty position at Naval Nuclear Power School in Orlando, FL, and is presently a faculty member in the Chemistry Department at the U.S. Naval Academy in Annapolis, MD. Mr. Campbell is currently a Ph.D. candidate in Chemical Physics at The Johns Hopkins University working under the direction of Professor Paul Dagdigian. His research interests involve the dynamics of chemical reactions, especially spin–orbit effects, and the role of reagent electronic excitation.

models are necessary for even a qualitative interpretation of the observed state selectivity.

This article is organized as follows. In the next section, we summarize the fine-structure splittings in the ground state and selected excited atomic states, concentrating on those atoms where spin–orbit effects have

TABLE I. Spin–Orbit Energies^a (in cm^{-1}) for the Ground Terms of Selected Atoms

atom	energies		
	Group IIIA (13)^b (np)		
	$^2P_{1/2}°$	$^2P_{3/2}°$	
B	0	16	
Al	0	112	
Ga	0	826	
In	0	2213	
Tl	0	7793	
	Group IVA (14) (np^2)		
	$^3P_0$	$^3P_1$	$^3P_2$
C	0	16	43
Si	0	77	223
Ge	0	557	1410
Sn	0	1692	3428
Pb	0	7819	10650
	Group VIA (16) (np^4)		
	$^3P_2$	$^3P_1$	$^3P_0$
O	0	158	226
S	0	397	574
Se	0	1989	2534
Te	0	4751	4707
	Group VIIA (17) (np^5)		
	$^2P_{3/2}°$	$^2P_{1/2}°$	
F	0	404	
Cl	0	882	
Br	0	3685	
I	0	7603	

^{a} Energies taken from ref 40. ^{b} Reference 236.

been studied. In section III, the various methods which have been employed to study reactions of individual spin–orbit states of both neutral atoms and ions are described and compared. We also consider the detection of spin–orbit states of product atoms. Section IV reviews the experimental data available on spin–orbit effects in chemical reactions, as well as the theoretical models used to interpret these results. While, strictly speaking, beyond the scope of this review, spin–orbit effects have also been observed in a variety of nonreactive collisional processes, including excitation transfer,[13-18] Penning ionization,[19-25] associative ionization,[26] charge-transfer collisions,[27-34] and electronic quenching.[35] Also relevant from the point of view of development of quantitative theoretical models for reactive processes is collisional transfer between atomic fine-structure states. The literature in this field is large, and several reviews are available.[36-38] Studies of nonreactive collisions will be mentioned here only when they are relevant for a reactive process.

II. Atomic Spin–Orbit States

Spin–orbit splittings arise from the interaction of the magnetic moments of the open-shell electrons with the effective magnetic field generated by the circulation of these electrons about the nucleus. Ignoring hyperfine structure, the total angular momentum $\vec{J}$ is given by the vector sum of the spin and orbital angular momenta $\vec{S}$ and $\vec{L}$, respectively, and hence, several levels of different J can arise from LS terms when both L and S are greater than zero. When Russell–Saunders coupling applies, the spin–orbit energy can be expressed[39] as

$$E_{so} = \frac{1}{2}A\{J(J + 1) - L(L + 1) - S(S + 1)\} \quad (1)$$

where the coupling constant A depends on the term. If A is positive, the level with the smallest value of J lies

TABLE II. Spin–Orbit Energies[a] (in cm^{-1}) for Metastable Terms of Selected Atoms

atom	energies			
	Group IIA (2)[b] ($nsnp$ or $nsnd$)			
	$^3P_0^\circ$	$^3P_1^\circ$	$^3P_2^\circ$	
Mg	21850	21870	21911	
Ca	15158	15210	15316	
Sr	14318	14504	14899	
	$^3D_1$	$^3D_2$	$^3D_3$	
Ba	9034	9216	9597	
	Group IIB (12) ($nsnp$)			
	$^3P_0^\circ$	$^3P_1^\circ$	$^3P_2^\circ$	
Zn	32311	32501	32890	
Cd	30114	30656	31827	
Hg	37645	39412	44043	
	Group VA (15) (np^3)			
	$^2D_{3/2}^\circ$	$^2D_{5/2}^\circ$	$^2P_{1/2}^\circ$	$^2P_{3/2}^\circ$
N	19231	19223	28840	28840
P	11362	11376	18722	18748
As	10592	10915	18186	18647
Sb	8512	9854	16396	18464
Bi	11419	15438	21661	33165
	Group I (1)			
	$(n+1)s$-$[3/2]_2^\circ$	$(n+1)s$-$[3/2]_1^\circ$	$(n+1)s'$-$[1/2]_0^\circ$	$(n+1)s'$-$[1/2]_1^\circ$
Ne	134044	134461	134821	135891
Ar	93144	93751	94554	95400
Kr	79973	80918	85192	85848
Xe	67068	68046	76197	77186

[a] Energies taken from ref 40. [b] Reference 236.

lowest in energy, and the multiplet is said to be normal, whereas, if A is negative, the multiplet is said to be inverted. For ground-state terms, normal multiplets arise from equivalent electrons when an incomplete subshell is less than half full; inverted multiplets arise from equivalent electrons in a more than half-filled subshell. For excited terms split by the spin–orbit interaction there are no general rules regarding the sign of A. In part, this is due to the influence of other effects, such as configuration interaction. It follows from eq (1) that the splittings between levels obey the Landé interval rule:

$$E(J + 1) - E(J) = A(J + 1) \qquad (2)$$

Deviations from this rule become particularly evident in heavier atoms where Russell–Saunders coupling no longer applies.

Of the main group elements, the ground state terms of atoms with electron configurations np, np^2, np^4, and np^5 exhibit spin–orbit coupling. The identity and energies of the fine-structure levels are listed in Table I. These splittings increase with increasing atomic number for a particular group in the periodic table. Russell–Saunders notation is often employed to designate the states even for heavy atoms, where spin multiplicity is no longer a rigorous label. As we shall see in the next section, a number of experimental techniques for the study of spin–orbit effects are facilitated by large splittings. However, in such cases, energetic effects can play an important role in the reaction dynamics. Excluded from consideration in Table I are the transition metal and rare earth elements, almost all of which exhibit fine-structure splitting in their ground terms.

Much of the experimental work on spin–orbit effects has actually involved metastable electronically excited atoms. Table II presents the spin–orbit energies for a selected list of these states, with emphasis on those
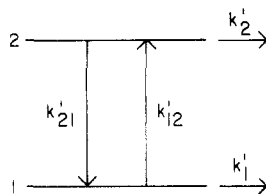
groups for which experiments are available. In Table II, the states of the inert gases are labeled as $(n + 1)$-$s[j]_J^\circ$, where j is the total angular momentum of the np^5 shell and J is the total angular momentum of the state. It should be noted that there is no designation for the spin of the state since spin is not a good quantum number for these states. In Paschen notation, these states are denoted $1s_5$ through $1s_2$, reading left to right across the columns in Table II. In LS coupling, these states would be described as $^3P_2^\circ$, $^3P_1^\circ$, $^3P_0^\circ$, and $^1P_1^\circ$; this notation is often employed, particularly for the optically metastable $J = 0$ and 2 levels.

III. Methods of Spin–Orbit State Selection and Detection

There have been a variety of experimental techniques utilized to study reactions of individual spin–orbit states. These fall into two categories of experimental methods, those which follow the collisional loss of the reactant states and those which monitor the formation of products. The former method is simple and widely applicable to many atoms. However, it suffers because the measured total collisional removal rate also includes nonreactive quenching processes for excited state reagents. The latter technique is advantageous for reactions having multiple reactive pathways since the spin–orbit effect on each of these can be investigated separately. This requires that the reagent spin–orbit states be selected by some means, for example, optical pumping state selection or selective collisional quenching. Each of these methods will be discussed and examples given in the following sections. In complementary experiments, the spin–orbit populations in atomic products have also been probed, for example by one-photon vacuum ultraviolet or two-photon laser fluorescence excitation and by observation of spontaneous infrared emission. Selected examples will be reviewed in section III.F. Slightly different techniques have been utilized for ion–molecule reactions; these are discussed in section III.E.

A. Time-Resolved Monitoring of Atomic States

A widely employed technique for the measurement of rate constants of individual atomic reagent states involves the measurement of atomic concentrations as a function of time after formation from a suitable precursor. The earliest version of this technique is flash photolysis,[41] in which the precursor is dissociated by irradiation from a pulsed flashlamp. Recent experiments have employed lasers as photodissociation sources. The concentrations of the various states are monitored by atomic absorption or fluorescence spectroscopy using atomic emission lamps as sources. A sufficient amount of inert gas must be added to ensure that the translational temperature is moderated back to the cell wall temperature in a time short compared to the time for reaction. With this detection technique it is necessary to verify the curve of growth, or the relationship between the measured absorption and atom concentration.[42,43] Alternatively, the spontaneous infrared emission from the spin–orbit excited state can be monitored as a function of time.[44-48] A recent innovation has been the use of an infrared laser to measure directly the population ratio of the ground and

Figure 1. Kinetic scheme for reactive and nonreactive processes in 2-level atoms.

Figure 2. Selected low-lying electronic states of the calcium atom. The wavelengths of radiative transitions are given in nm.

spin–orbit-excited states of bromine and iodine by observation of the gain or absorption of the probe laser beam.[49-52] Diode and F-center lasers[49,50] are particularly useful because they can be tuned across the hyperfine lines and can also yield velocity information from Doppler analysis.

While this technique has been widely used to measure rate constants involving reactions of electronically excited atoms,[12,53,54] in favorable cases it has also been possible to study reactions of individual spin–orbit states. This is feasible when the collisional intramultiplet mixing rate is slow, as would be expected in atoms with large fine-structure splittings. To illustrate the applications and limitations of this technique, we describe its application to atoms with two fine-structure levels, such as is found in reactions involving halogen atoms.

Figure 1 presents the kinetic scheme appropriate to the halogens and other 2-level atoms, e.g., In and Tl. The time dependence of the atomic concentrations n_1 and n_2 are governed by the following equations:

$$dn_1/dt = -n_1(k_1' + k_{12}') + n_2 k_{21}' \qquad (3a)$$

$$dn_2/dt = -n_2(k_2' + k_{21}') + n_1 k_{12}' \qquad (3b)$$

Here k_1' and k_2' are the pseudo-first-order rate constants for removal of the relevant atomic states by reaction, quenching, or collision on the walls, and k_{12}' and k_{21}' are the corresponding nonreactive collisional transfer rates between the two levels. Each of these rates can be written as

$$k' = nk + \kappa \qquad (4)$$

where n is the reagent density, k is a bimolecular rate constant, and κ represents the removal rate by other processes. It should be noted that k_{21} and k_{12} are related by microscopic reversibility.

Equation 3 is most easily discussed by considering two limiting cases, for which k_{21}' and k_{12}' are (a) large and (b) small. In the former regime, the two levels are rapidly brought into equilibrium, and the removal rates for both are identical with and equal to an "apparent" loss rate k_{app}':

$$k_{app}' = k_2'[k_{12}'/(k_{21}' + k_{12}')] + k_1'[k_{21}'/(k_{21}' + k_{12}')] \qquad (5)$$

$$= (K_{eq}k_2' + k_1')/(1 + K_{eq})$$

with the equilibrium constant $K_{eq} = k_{12}'/k_{21}'$. It is obvious that spin–orbit effects will be totally obscured here.

On the other hand, if the upward rate k_{12}' is slow, for example, because of a large energy spacing between the levels, then the population in state 2 will decay exponentially with an apparent rate constant $k_2' + k_{21}'$. In addition, if the second term on the right-hand side of eq 3a can be neglected because of a higher population
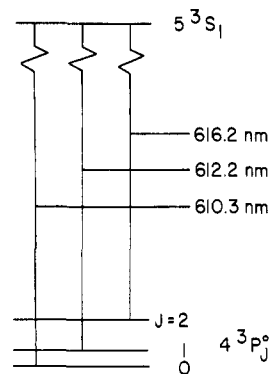
in state 1 than in state 2, then state 1 will also decay exponentially with rate k_1'. We also require that the cascade from higher excited states possibly formed in the photolytic preparation be negligible. By measurement of the decay rates of the two states vs. reactant density, the bimolecular rate constants $k_2 + k_{21}$ and k_1 can be determined. Differences in these two rates can then be ascribed to spin–orbit effects, provided that the nonreactive quenching term k_{21} is negligible, which is often not the case. The clearest situation occurs when the lower level is removed at a faster rate than the upper level. Otherwise, the branching ratio between reactive and nonreactive decay of state 2 is required for an unambiguous assessment of the magnitude of the spin–orbit effect.[46,47,55]

Spin–orbit effects have also been observed in reactions in flow systems.[14,56-61] Here the reaction time is equated with the distance along a flow tube. In general, however, the flow technique[43,62-64] is less suitable unless the reagent states are selected by optical or kinetic means, as we describe in the next two sections. Unlike techniques which follow the reactants in real time, here the initial spin–orbit populations usually follow the Boltzmann distribution, and study of the excited states is rendered more difficult because of a small population in these states.

B. Optical Excitation or Depletion

State selection by optical methods has become a rather general and versatile tool. The general principles are presented in detail along with selected applications in a forthcoming book,[65] as well as in other places.[38,66-69] Optical selection can be used in both beam and bulb experiments to prepare specific excited levels by excitation or to deplete a selected level by optical pumping. The latter technique has been used to investigate spin–orbit effects in reactions involving a number of atoms including $Ca(^3P^\circ)$,[70-73] $Sr(^3P^\circ)$,[74] $Ba(^3D)$,[75] and $Ar(^3P_2^\circ, {}^3P_0^\circ)$.[18,76] One particular advantage of state selection of the reagents is that spin–orbit effects on the product-state distributions of specific reaction pathways can be observed.

The optical pumping-state selection technique can be illustrated by the calcium atom,[70,72] whose relevant energy levels are displayed in Figure 2. The spin–orbit state distribution in the metastable $^3P^\circ$ manifold can be altered by irradiation of a metastable Ca* beam on one of the lines of the $5\ ^3S_1 \leftarrow 4\ ^3P_J^\circ$ multiplet near 610 nm. The population of the pumped $^3P_J^\circ$ level is redistributed among the other fine-structure states by

spontaneous decay from the ^3S level. The power density of a single-mode cw dye laser beam of 50 mW and diameter of 4 mm was sufficient to reduce the population of a given level to less than 5% of its original magnitude. Since a substantial fraction of the excited-state decay returns the atoms to the pumped level, many pump cycles are required for depletion. In order to insure that all atoms are pumped, the line width of the pump transition, which will usually be dominated by power broadening, should be greater than the Doppler width. Thus, the pump line width dictates the degree of beam collimation required in a given experiment. Line-width considerations will also limit the degree of depletion attainable in atoms with hyperfine structure, for example, the odd isotopes of Sr and Ba.[77] Weissmann et al.[78] have described a simple standing-wave multimode dye laser with a wide intracavity space. This device allows simultaneous pumping of all isotopes over a 10-GHz bandwidth with narrow (63 MHz) mode separation and high intracavity power density.

Since the other, unpumped, spin–orbit populations are usually modulated by the optical pumping process, determination of reactive cross sections for individual spin–orbit levels requires knowledge of the populations of all the levels when the pump laser is tuned to each of the transitions. These can be determined by fluorescence excitation measurements[79,80] with a second dye laser.

To determine reaction cross sections σ_J for a specific reagent spin–orbit level J, the change in signal S monitoring a product must be measured.[70] With the pump laser off, the signal is given by

$$S_{off} = k\sum_J n_J{}^{off}\sigma_J = k\sigma_{av} \tag{6}$$

where the $n_J{}^{off}$ represent the relative reactant spin–orbit populations in the unpumped case, and k is a proportionality constant which includes the absolute reagent number densities, detector efficiency, and geometrical viewing factors, etc. The quantity σ_{av} represents the reaction cross section averaged over the incident spin–orbit distribution.

When the pump laser is tuned to the ith pump transition, the product signal changes by a factor R_i, and the observed signal can be expressed as

$$S_i = R_i S_{off} = k\sum_J n_J{}^i\sigma_J \tag{7}$$

where the relative reagent spin–orbit populations are now given by $n_J{}^i$. Dividing eq 7 by eq 6, we have

$$R_i = \sum_J n_J{}^i(\sigma_J/\sigma_{av}) \tag{8}$$

which yields a set of equations for the unknown cross-section ratios (σ_J/σ_{av}), which can be determined by measurement of the ratios R_i. The cross sections σ_J can be put on an absolute scale by separate experiments to measure the magnitude of σ_{av}. In some situations, particularly where only two spin–orbit levels need to be considered, it may be more convenient to solve directly for the ratio of the spin–orbit dependent cross sections, e.g., σ_0/σ_2 for $^3P_0{}^\circ$ and $^3P_2{}^\circ$ reagents in Sr*[74] or Ar*.[18,76]

One possible complication in optical pumping-state selection is the possibility of generating coherence and/or alignment in the pumped atoms. Such effects have been extensively studied in bulb experiments.[69]

Yuh and Dagdigian[81] carried out a density matrix calculation of the state selection process in Ca($^3P^\circ$). They concluded that no coherences or alignment were generated in their experiments because of the mixing of M levels by the earth's magnetic field and the efficient averaging due to the spread in beam velocity. In an examination of optical pumping of metastable neon atoms, Kroon et al.[68] showed experimentally that a weak magnetic field is required for removal of all the M levels by pumping with a polarized laser.

The principal factor limiting the application of optical pumping state selection is the relatively limited wavelength range of cw dye lasers, although cw frequency-doubled radiation at moderate powers is now available.[82] In principle, the use of pulsed laser radiation, with the associated wider wavelength coverage, would extend the number of atoms to which optical pumping could be applied. However, the depletion attainable would be incomplete because typical laser pulse widths are usually shorter than atomic radiative lifetimes. A simple two-state model (equal upper and lower level degeneracies) for the saturation of ground and excited levels during the laser pulse suggests an upper limit of 50% depletion of the pumped level.

Direct optical excitation with lasers can be employed for the preparation of specific radiating excited atomic states. This technique has been extensively utilized for the study of nonreactive collision processes in a number of atoms including the lowest $^2P^\circ$ and ^2D states of the alkali atoms,[83–97] the $np^5(n+1)p$ configuration of the rare gases,[21,98,99] the 5 $^1P^\circ$ and 6 ^1S states of calcium[100–103] and the $3d^54p$ $^7P_J{}^\circ$ multiplet of chromium.[104] In a few cases, chemical reactions of radiating excited species have been investigated both by one-step[105] and two-step[106] laser irradiation although spin–orbit effects have not been explored. Two-photon pulsed laser excitation of the $J = 0$ and 2 levels of the $5p^56p$ manifold of xenon has recently been utilized for the study of reactions of these states with halogen donors,[107] as well as for the measurement of nonreactive energy transfer rates.[108]

Because of the need to create a high steady-state population in the excited state for many experiments, one spin–orbit level is often more convenient for study. For example, in the Na 3 $^2P^\circ$ multiplet a high fractional population can be maintained in the $^2P_{3/2}{}^\circ$ level by pumping on the 3 $^2P_{3/2}{}^\circ$, F = 3 ← 3 $^2S_{1/2}$, F = 2 hyperfine transition.[38,109–112] Population does not leak to other states since the excited state can radiatively decay only to the pumped state.

Optical excitation also creates a nonuniform M distribution in the excited level. The investigation of polarization and coherence effects in molecular collisions has evoked great interest,[21,38,69,92,95–99,103,105,112–115] but this subject is beyond the scope of this review. Such effects need to be considered in extracting degeneracy-averaged information from such experiments. Nevertheless, it can be anticipated that laser excitation will soon be employed to study spin–orbit effects in reactions involving excited atomic states. Excitation with a resonance lamp has already been used to compare the rate constants and branching fractions of several reactions of the radiating $^3P_1{}^\circ$ state of Xe and Kr relative to those of the metastable $^3P_2{}^\circ$ state.[116,117]

Stimulated emission pumping[118–120] has recently been employed for state selection of iodine atoms.[121] Here,

an iodine atom laser (the "dump") operating on the $^2P_{1/2}{}^\circ \rightarrow {}^2P_{3/2}{}^\circ$ transition at 1315 nm causes the radiative decay of the excited spin–orbit state to the ground state. Reactions of the individual states can be studied by comparison of signals without and with the dump laser on. Thus far, this technique has been used to study iodine atom recombination reactions.

C. Selective Collisional Quenching or Production

In favorable cases, the spin–orbit dependence of the rate of nonreactive collisional processes may be used for spin–orbit selection of the reactant atoms. For example, it is known that metastable $Ar(^3P_2{}^\circ)$ is quenched by krypton much more efficiently than is $Ar(^3P_0{}^\circ)$: $k_2(Kr)/k_0(Kr) = 18 \pm 2.^{13,17,122}$ On the other hand, the opposite ordering of quenching efficiency applies to CO: $k_0(CO)/k_2(CO) = 8 \pm 1.^{14,122}$ The addition of Kr or CO to flows of metastable argon atoms has been utilized to prepare nearly pure metastable argon in the $^3P_0{}^\circ$ or $^3P_2{}^\circ$ states, respectively.[122] As with the optical selection methods described in the last section, this allows the observation of product channels from reaction of the individual spin–orbit reagent states.[60,123] The present method requires that possible reactions of any metastable collisionally excited states of the quench molecule be taken into account.

In some cases, the reactions of individual spin–orbit states can be determined by comparing the signals resulting from a mixture of reagent spin–orbit states to those in which the reagents have been collisionally quenched to the lowest spin–orbit state of the manifold. For example, it is known that N_2 selectively quenches the $Hg(^3P_2{}^\circ)$ state to the $Hg(^3P_{0,1}{}^\circ)$ states, rather than to the ground $Hg(^1S)$ state.[124,125] Since the J = 1 spin–orbit state radiatively decays rapidly to the ground electronic state, the addition of N_2 to a flow of metastable atoms will convert the mixture of $Hg(^3P_{0,2}{}^\circ)$ to pure $Hg(^3P_0{}^\circ)$. This technique has been used in both beam[126,127] and flow[61] experiments to study the reactions of the individual spin–orbit states of metastable mercury atoms. A similar method has also been applied to the study of the individual states of metastable inert gases.[63]

Spin–orbit selectivity in the excitation of a multiplet may, in principle, also be used to study collisional processes of individual states. For example, the J = 0 to 2 population ratio in metastable $Hg(^3P_J{}^\circ)$ formed by electron impact excitation has a significant variation with electron energy.[128] This preparation method has been used in the study of reactive[129] and nonreactive[128,130] collisions of $Hg(^3P_{0,2}{}^\circ)$. However, only lower limits to $^3P_0{}^\circ$ cross sections could be obtained, in part because of the small $^3P_0{}^\circ$ population and the small ratio of $^3P_0{}^\circ$ to $^3P_2{}^\circ$ cross sections.

D. Miscellaneous Methods

Since the spin–orbit splitting in atomic fluorine is comparable to kT, variation of the temperature of a F atom source was utilized to vary the relative spin–orbit populations.[131] In order to change the temperature without substantially altering the laboratory velocity, an effusive source of fluorine, which was prepared by thermal dissociation of F_2, was employed. In principle, a variable-temperature supersonic source could be used if the seed gas mixture were varied to keep the velocity

constant as the temperature was changed. Ideally, the spin–orbit population ratio should also be monitored to check for possible spin–orbit relaxation in the supersonic expansion.

For paramagnetic atoms, magnetic state selection[132] allows manipulation of the spin–orbit population in an atomic beam. Since the deflection is proportional to the magnetic quantum number M, application of an inhomogeneous magnetic field (e.g., Stern–Gerlach magnet) will remove all atoms from the beam except those for which $M = 0$. By comparison of the signals with the deflecting magnet on and off, this method was used to measure quenching cross sections for the $^3P_2{}^\circ$ state of metastable argon.[133] Knowledge of the $^3P_2{}^\circ$ to $^3P_0{}^\circ$ population ratio then allowed extraction of $^3P_0{}^\circ$ cross sections. In this method, since the cross sections can depend upon the orientation, the M-state distribution should be scrambled prior to reaction to disentangle orientational and spin–orbit effects.

E. Methods Applicable to Ions

Photoionization is the cleanest method for the preparation of reactant ions with well characterized distributions of internal states. This technique has been used to study reactive and nonreactive charge-transfer collisions of the $^2P_{3/2,1/2}{}^\circ$ spin–orbit states of the argon ion.[27-32] Here, Ar^+ in the lowest $^2P_{3/2}{}^\circ$ spin–orbit state can be prepared by irradiation of the parent gas at the vacuum ultraviolet wavelength (approximately 78.7 nm) corresponding to the ionization threshold. At wavelengths below 77.8 nm, production of both spin–orbit states becomes energetically allowed. In the threshold electron–secondary ion coincidence (TESICO) method, the different internal states of the ion are distinguished by detecting only those ions which are produced in coincidence with electrons of low kinetic energy.[134] Thus, for a given vacuum ultraviolet wavelength, the internal energy of the ions under consideration is specified by energy conservation in the ionization process. The ions are drawn out of the production zone, allowed to react with a static target gas, and the product and unreacted incident ions are drawn out and mass analyzed. The relative collision energy can be changed by variation of the reagent ion extraction potentials. This technique has been used to study the spin–orbit dependence of the $Ar^+ + H_2$ reaction[27,29] and several charge transfer processes.[28,32]

Recently, state-selective ion preparation has also been employed in a crossed-beam apparatus.[30,31] Here Ar^+ ions in the lowest $^2P_{3/2}{}^\circ$ state or a known mixture of $^2P_{3/2}{}^\circ$ and $^2P_{1/2}{}^\circ$ states are formed by vacuum ultraviolet irradiation of a supersonic beam of argon. The ions are extracted and then crossed with a second supersonic beam of the neutral collision partner. The state composition of the reactant beam vs. ionizing wavelength is known from a previous photoelectron spectroscopy study of the ionization of argon.[135] In this method it is important to maintain a low pressure in the photoionization chamber since the purity of the reactant ion beam was found to be affected by high background pressure. This also suggests collisional equilibration in the ionization region could affect the state selectivity in the TESICO method. In a study of the $Ar^+ + Ar$ symmetric charge transfer process,[30] the spin–orbit state of the product ions was determined by

utilizing the spin–orbit dependence of the $Ar^+ + H_2$ reaction.

Near-resonant charge transfer between CO^+ and Kr has also been used to prepare a nearly pure $Kr^+\ ^2P_{3/2}{}^\circ$ beam in order to study the spin–orbit dependence of the $Kr^+ + H_2$ reaction in an ICR experiment.[33] The purity of the beam was checked by using the charge-transfer reaction of Kr^+ with CH_4. Because of the 1-eV spin–orbit splitting in Kr^+, this charge-transfer reaction is endoergic for the $^2P_{3/2}{}^\circ$ state but exoergic for $^2P_{1/2}{}^\circ$ so that the amount of ionized methane product detected is an indication of the purity of the $Ar^+\ ^2P_{3/2}{}^\circ$ beam.

The biexponential decay of reactant Ar^+ ions vs. the density of added neutral gas, which has been observed in a drift experiment in a number of reactions, has been ascribed to the differing reactivities of the $^2P_{3/2}{}^\circ$ and $^2P_{1/2}{}^\circ$ states.[136] These data have been utilized to extract reaction rate constants for the two spin–orbit states. This indirect method for studying spin–orbit dependence has, however, been criticized.[137]

F. Detection of Product Spin–Orbit States

A number of spectroscopic methods have been applied to the measurement of spin–orbit populations of atomic reaction products. These have almost exclusively involved the halogen atoms but are in principle applicable to other atoms.

The production of excited $^2P_{1/2}{}^\circ$ bromine or iodine atoms has been investigated both by time-resolved[45–47] and steady-state flow[138–145] experiments through the spontaneous $^2P_{1/2}{}^\circ \rightarrow\ ^2P_{3/2}{}^\circ$ emission in the infrared. However, because of the relatively small radiative decay rates ($A_{I*} = 8\ s^{-1}$ [146,147] and $A_{Br*} = 0.89\ s^{-1}$ [148]), this emission is weak and relatively difficult to detect. Since the emission intensity is a measure of the excited state population only, the relative yield of spin–orbit-excited $Br*$ atoms in the $I* + Br_2$ reaction was derived from measurement of the relative reactant $I*$ and product $Br*$ emission intensities, corrected for detector wavelength response and the transition probabilities.[46,47] In these bulb experiments, it was also necessary to take account of collisional deactivation. In low-pressure flow experiments, the $Br*$ or $I*$ product yield could be determined by comparison of the halogen infrared emission intensity with that of a hydrogen halide reaction product from the reaction under study[138–143] or from a reference reaction.[144,145] Measurement of the gain or absorption of radiation from a halogen atom laser operating on the $^2P_{1/2}{}^\circ \rightarrow\ ^2P_{3/2}{}^\circ$ transition has also been used to estimate the spin–orbit population ratio.[51,52]

Ground and spin–orbit-excited atoms produced in chemical reactions have been monitored by time-resolved resonance absorption spectroscopy in the vacuum ultraviolet[149,150] in a manner entirely analogous to that used to follow the collisional removal of reactant atoms. Laser techniques have also been applied to the detection of atoms by fluorescence excitation. Ground- and excited-state Br have been monitored in a crossed beam experiment[131] by excitation with coherent vacuum ultraviolet radiation produced by frequency mixing.[151]

There has been considerable interest in the development of 2-photon excitation schemes for the detection of atoms in order to avoid the use of vacuum ultraviolet light. Most of the atoms on the right-hand side of the periodic table have now been detected by 2-photon
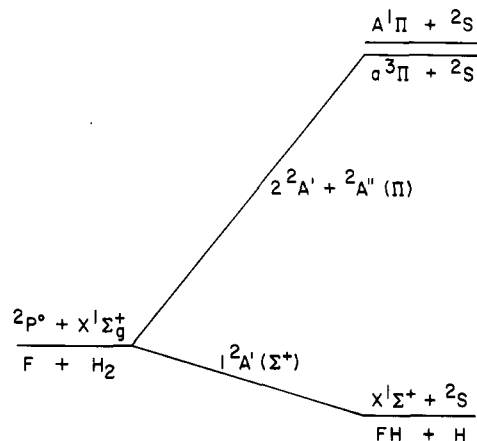

**Figure 3.** Adiabatic correlation diagram for the $F + H_2$ reaction.

fluorescence excitation.[152–158] Since the excited state is of the same parity as the ground state, it radiatively decays in two steps, first by visible (or infrared) emission to a lower state (usually the first resonance level) and then by vacuum ultraviolet decay back to the ground state. In many excitation schemes, the visible fluorescence is the emission detected. This technique has been used to determine the spin–orbit-state population ratio in iodine atoms formed in a number of reactions of fluorine atoms with iodine-containing molecules.[159,160]

Finally, if the spin–orbit splitting is large enough, it is possible to distinguish these states in a translational energy-angle flux contour plot of a crossed-beam reaction, as has been done for the $Kr^+(^2P_{3/2,1/2}{}^\circ)$ product in the $Hg^{2+} + Kr$ charge exchange process.[34]

## IV. Experimental Results

A. Halogen Atoms

Considerable effort has been devoted to the study of spin–orbit effects in reactions involving halogen atoms, both with regard to the reactivity of the ground $^2P_{3/2}{}^\circ$ and excited $^2P_{1/2}{}^\circ$ states and the formation of the individual spin–orbit states of halogen atom products. Reactions studied include those involving halogen atoms with hydrogen halides and halogen molecules:

$$X + HY \rightarrow HX + Y \tag{9}$$

$$X + YZ \rightarrow XY + Z \tag{10}$$
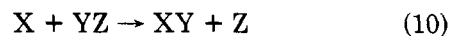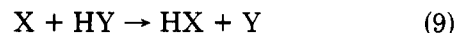
In addition, the $F + H_2$ reaction has been investigated in several theoretical studies.

Because of the hole in the outer p subshell, three electrostatic surfaces arise from the interaction of a halogen atom with a molecule in arbitrary C_s geometry. The adiabatic correlation of these surfaces is indicated in Figure 3 for the prototype $F + H_2$ reaction. In valence bond terminology, the surface corresponding to the hole in the triatomic plane ($1\ ^2A'$) leads to reaction, while the two out-of-plane orientations result in repulsive interactions and connect to energetically inaccessible electronically excited products. When the spin–orbit interaction is included, the doubly degenerate $^2P_{1/2}{}^\circ$ state correlates with the $2\ ^2A'$ surface, while the quadruply degenerate lower $^2P_{3/2}{}^\circ$ state correlates with the reactive $1\ ^2A'$ and unreactive $^2A''$ surfaces. We note that the character of the wave function must
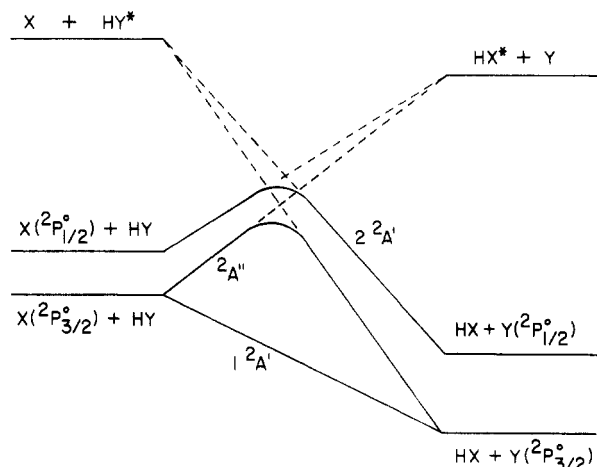
Figure 4. Correlation diagram for X + HY reactions. The $^2A''$ and 2 $^2A'$ orbitally correlate with highly excited Π states of HY and HX.

change as the reactants approach since the p hole has a preferred orientation for each of these electrostatic surfaces, while there can be no such preference in the isolated atom. In spectroscopic terms, the isolated reactants follow Hund's case (e) coupling,[161] wherein neither $\vec{L}$ nor $\vec{S}$ is strongly coupled to a body-fixed axis; the specification of an electrostatic surface when the reagents are strongly interacting implies a Hund's case (a) representation.

The discussion above suggests that if nonadiabatic effects are unimportant, then the less-energetic $^2P_{3/2}°$ state will be more reactive. This expectation is confirmed in a number of theoretical studies of the F + H_2 reaction. In a semiclassical study using diatomics-in-molecules (DIM) surfaces, Tully[162] found that the reactive cross sections were 10 times larger for the $^2P_{3/2}°$ than for the $^2P_{1/2}°$ initial state. A comparable result was found by Komornicki, Morokuma, and George[163] with a similar semiclassical technique and by Last and Baer[164] in a collinear quantum mechanical calculation. Quantum mechanical calculations on the nonreactive channel[165,166] indicate the importance of resonant electronic-to-rotational energy transfer in the collisional removal of the excited $^2P_{1/2}°$ state because of a match of the F atom fine-structure splitting and H_2 rotational spacings:

$$F\left(^2P_{1/2}°\right) + H_2(J = 0) \rightarrow F\left(^2P_{3/2}°\right) + H_2(J = 2) \quad (11)$$
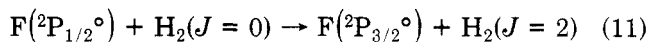
In a high-resolution crossed molecular beam study by Lee and co-workers,[167] no HF reaction product attributable to the $^2P_{1/2}°$ reactant state was detected. This reaction pathway would be observable here since some portion of the additional 1.16 kcal/mol available energy would appear as product translation.

In reactions 9 and 10, all three electrostatic surfaces arising from the reactants correlate with the lowest electronic configurations of the products. Nevertheless, as shown in Figure 4, two of the surfaces orbitally correlate with excited products and hence are likely to possess significant barriers.[44] From a consideration of the long-range behavior of the $^2A''$ and 2 $^2A'$ surfaces, Das et al.[159] claim that the former should be more repulsive. The product halogen atom spin–orbit state distribution is also of interest in these reactions. In the absence of nonadiabatic effects, the $^2P_{1/2}°$ state would be formed by collisions proceeding on the 2 $^2A'$ surface.

Significant spin–orbit effects have been found in reactions of type 9 and 10, as expected from the diagram in Figure 4. In a study of the Br + HI reaction, Bergmann et al.[44] obtained evidence that the ground $^2P_{3/2}°$ state was at least 4 times more reactive than spin–orbit-excited bromine. Moreover, it was found that Br* reagent was removed primarily by nonreactive processes.[50] Polanyi and co-workers[131] carried out an extensive crossed beam study of the F + HBr reaction as a function of collision energy. The reagent F atom spin–orbit population was varied by changing the temperature of the source. From the insensitivity of the product Br atom spin–orbit distribution to the incident F*/F ratio, they concluded that there is a substantial barrier to the adiabatic process F* + HBr → HF + Br*.

The removal rates for collisions of halogen atoms in the $^2P_{1/2}°$ state with various halogen molecules have been measured by a number of different investigators. The derived bimolecular rate constants, strictly speaking, include both chemical reaction and nonreactive quenching, as discussed in section III.A. In many cases, the corresponding $^2P_{3/2}°$ chemical reaction is endothermic so that possible spin–orbit effects are obscured by trivial energetic constraints.[169,170] A particularly clear example, however, is the Br + IBr → Br_2 + I reaction, which is exothermic for both reactant states. In a recent study utilizing infrared F-center laser gain and absorption, Haugen, Weitz, and Leone[50] determined the following room temperature rate constants for this reaction:

$$k\left(^2P_{3/2}°\right) = (4.2 \pm 0.5) \times 10^{-11} \text{ cm}^3 \text{ molecule}^{-1} \text{ s}^{-1} \quad (12a)$$

$$k*\left(^2P_{1/2}°\right) = (1.9 \pm 0.4) \times 10^{-12} \text{ cm}^3 \text{ molecule}^{-1} \text{ s}^{-1} \quad (12b)$$

These values are in good agreement with previous measurements of k and $k*$ by Clyne and Cruse,[168] Hofmann and Leone,[46] and Gordon et al.,[51] while the results from an early study by Donovan, Hathorn, and Husain[169] differ significantly. Even neglecting the contribution of quenching to $k*$, it can be seen that the lower $^2P_{3/2}°$ state is significantly more reactive.

A number of workers[47,169-172] have studied the reaction $I(^2P_{1/2}°) + Cl_2 \rightarrow ICl + Cl$ ($^2P_{3/2,1/2}°$), which is endoergic for the ground-state I reactant. The very small rate constant ($\sim 6 \times 10^{-15}$ cm^3 molecule^{-1} s^{-1}) indicates a significant barrier along the 2 $^2A'$ surface and a small nonadiabatic transition probability to the 1 $^2A'$ and $^2A''$ surfaces. Lilenfeld et al.[172] present evidence that the primary Cl product is the ground $^2P_{3/2}°$ state, indicating that the reaction channel proceeds predominantly in a nonadiabatic fashion. By contrast, the reverse Cl + ICl → I + Cl_2 reaction has been studied by Clyne and Cruse.[168] In this case, the excited state $^2P_{1/2}°$ reactant is more reactive than the ground state, with $k*/k \simeq 3.7$. However, this result has recently been questioned.[172]

A number of studies have focused on the determination of the spin–orbit-state distribution of product halogen atoms. In part, the motivation of these investigations has been to test the importance of the adiabatic pathway on the 2 $^2A'$ surface between spin–orbit excited reagents and products. Table III summarizes the results of these experiments. It can be seen that there is considerable variation in the observed

TABLE III. Halogen Atom Product Spin-Orbit-State Ratios

reaction	$X(^2P_{1/2}°)/X(^2P_{3/2}°)$	method	ref
$F + HCl \rightarrow HF + Cl$	0.10	VUV absorption	173
$F + HBr \rightarrow HF + Br$	0.07 ± 0.03	infrared emission	141
	0.10 ± 0.04	infrared emission	142
	0.056 ± 0.004[a]	VUV LIF	131
$F + DBr \rightarrow DF + Br$	0.0101 ± 0.0016	VUV LIF	131
$F + HI \rightarrow HF + I$	<0.02[b]	infrared emission	138
	<0.005[b]	infrared emission	142
	0.5	VUV absorption	150
	<0.01	2-photon LIF	159
$F + Br_2 \rightarrow BrF + Br$	<0.01[b]	infrared emission	144
$F + I_2 \rightarrow IF + I$	<0.0004[b]	infrared emission	144
	<0.01[b]	2-photon LIF	159
	0.03	infrared emission	145
$F + ICN \rightarrow FCN + F$	<0.015[b]	2-photon LIF	159
$F + CH_3I \rightarrow CH_3F + I$	0.42 ± 0.14	2-photon LIF	160
$F + C_2H_5I \rightarrow C_2H_5F + I$	0.32 ± 0.13	2-photon LIF	160
$F + i\text{-}C_3H_7I \rightarrow i\text{-}C_3H_7F + I$	0	2-photon LIF	160
$Cl + HI \rightarrow HCl + I$	<0.005[b]	infrared emission	139
$I^*(^2P_{1/2}°) + Br_2 \rightarrow IBr + I$	~4	VUV absorption	149
	>5.7	laser gain/absorption	181
	~6	laser gain/absorption	51
$H + HI \rightarrow H_2 + I$	<0.02[b]	infrared emission	174
$H + BrCl \rightarrow HCl + Br$	<0.004[b]	infrared emission	140
$H + Br_2 \rightarrow HBr + Br$	<0.01[b]	infrared emission	175
$H + ICl \rightarrow HCl + I$	~0.001	infrared emission	140
	0	infrared emission	176
$H + IBr \rightarrow HI + Br$	<0.08	laser gain/absorption	52
$\rightarrow HBr + I$	<0.15	laser gain/absorption	52

[a] Value at room temperature. Ratio declines slightly with increasing collision energy. [b] Upper limit. No X* observed.

X^*/X product ratio, although in most cases the ground $^2P_{3/2}°$ state is preferentially populated. In some reactions, formation of the $^2P_{1/2}°$ state is forbidden by energetic considerations; however, this does not apply to any of the reactions listed in Table III. There are some disagreements between different studies of the same reaction. The most serious of these involves the F + HI reaction. Here Burak and Eyal[150] derived the ratio $I^*/I \simeq 0.5$, while a very low spin-orbit population ratio was found in three other experiments.[138,142,159] An information theoretic analysis[177] using the experimental HF vibrational distribution predicted a statistical ratio $I^*/I = 0.5$. The preponderant direct experimental evidence indicates a low spin-orbit ratio for this reaction.

There are also differences in the determined I^*/I ratio for the $F + I_2 \rightarrow IF + I$ reaction. By comparing the infrared emission from I* and HF $\Delta v = 2$ emission from $F + H_2$, Brunet et al.[145] derive a ratio of 0.03. No I* emission was observed by Agrawalla et al.[144] in a similar type of experiment. In addition, no I* product was detected by Das et al.[159] by 2-photon laser fluorescence excitation. The reasons for these differences are not obvious, but nonetheless it is clear there is little iodine product spin-orbit excitation in this reaction. Trickl and Wanner[178] observed bimodal IF vibrational distributions from the $F + I_2$, IBr, and ICl reactions. They inferred that the two peaks could be identified with branching into the two iodine spin-orbit states since trajectory calculations[179] on LEPS surfaces could not reproduce the low v component. Their conclusion of a large I^*/I ratio in these reactions is not substantiated by direct measurement, and an alternative explanation for the bimodal distribution must be sought.

It has been assumed[51,180] that excited $^2P_{1/2}°$ product is formed by adiabatic collisions from excited $^2P_{1/2}°$ reagents along the 2 $^2A'$ surface. For F atom reactants, for which the room temperature Boltzmann $^2P_{1/2}°$ to

$^2P_{3/2}°$ ratio is 0.07, this would imply a spin-orbit ratio of about this value in the halogen atom products. Ratios close to this value have been found[131,141,142,173] for the F + HCl and HBr reactions at room temperature; but other fluorine atom reactions show drastically different results. In fact, for the F + HBr reaction, Hepburn et al.[131] concluded that Br* product is formed by nonadiabatic processes from the $^2P_{3/2}°$ reactant: No dependence of the Br*/Br product ratio on the reagent F*/F ratio was found. Since the $^2A''$ surface is expected to be repulsive, Br* products are assumed to be formed by interaction of the 1 $^2A'$ and 2 $^2A'$ surfaces in the exit channel.

In cases where the barrier on the 2 $^2A'$ surface is small, adiabatic formation of spin-orbit excited product is possible. The $I^* + Br_2 \rightarrow IBr + Br^*$ reaction is a good example of this. Houston,[45] Wiesenfeld and Wolk,[55,149] Spencer and Wittig,[181] and Gordon et al.[51] demonstrated a high correlation of product Br* with reactant I*. The earlier infrared fluorescence measurements of Hofmann and Leone[47] by contrast indicated a much smaller yield. Weisenfeld and Wolk[55,149] have determined branching ratios of the reactive and nonreactive channels by vacuum ultraviolet absorption spectroscopy of the product atoms and found that ~80% of the reactive collisions yielded Br* product. The studies by Spencer and Wittig[181] and Gordon et al.[51] using laser gain/absorption experiments found the branching ratio to be even larger; however, these latter experiments have been criticized[50] for neglecting the selective ground state depletion from the reaction $Br(^2P_{3/2}°) + IBr \rightarrow Br_2 + I$ which would significantly enhance laser gain. The diode gain/absorption experiments by Haugen et al.[50] found no evidence that the secondary reaction Br + IBr was a problem in the measurements by Wiesenfeld and Wolk.[149]

Gordon et al.[51] presented evidence for a strong correlation between reactant and product spin-orbit ex-

cited state in the F + Br_2 reaction based on the observation that the Br product spin–orbit population ratio is found to be sensitive to the photolytic fluorine atom precursor used, presumably because the different precursors yield different fractions of excited-state F atoms. An intriguing reaction is the gas-phase Walden inversion F + RI → RF + I. Reactions with R = CH_3, CH_3CH_2, i-C_3H_7, and t-C_4H_9 were studied[160] in a flow system using two-photon laser-induced fluorescence for detection of the I atoms. The I*/I ratio was found to be large for R = CH_3 but decreases as the size of the alkyl group increases.

We thus observe a variety of dynamical behavior in the reactions of halogen atoms. The spin–orbit effect in a particular reaction will depend on the reaction exoergicity, the existence of potential barriers to reaction especially for $^2P_{1/2}°$ reagents, and the role of nonadiabatic effects. In general, however, the $^2P_{3/2}°$ reagent is found to be more reactive than the excited $^2P_{1/2}°$ state, and halogen atom products are usually preferentially formed in the ground $^2P_{3/2}°$ state.

B. Inert Gases
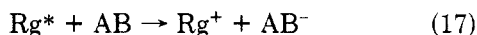
1. Metastable Excited Atoms

Collision processes involving metastable excited inert gas atoms have been the object of numerous studies, in part because the large electronic energy enables a number of different decay pathways to occur.[63,182,183] These include excitation transfer
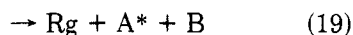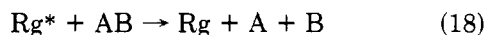
$$Rg^* + AB \rightarrow Rg + AB^* \qquad (13)$$
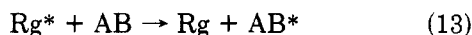
Penning, associative, and dissociative ionization,

$$Rg^* + AB \rightarrow Rg + AB^+ + e^- \qquad (14)$$

$$\rightarrow RgAB^+ + e^- \qquad (15)$$

$$\rightarrow Rg + A^+ + B + e^- \qquad (16)$$
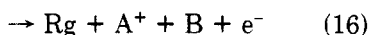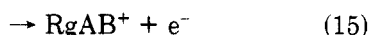
ion pair formation,

$$Rg^* + AB \rightarrow Rg^+ + AB^- \qquad (17)$$

molecular dissociation, possibly accompanied by electronic excitation,

$$Rg^* + AB \rightarrow Rg + A + B \qquad (18)$$

$$\rightarrow Rg + A^* + B \qquad (19)$$

as well as excimer formation, the only pathway which can be described as a chemical reaction:

$$Rg^* + AB \rightarrow RgA^* + B \qquad (20)$$
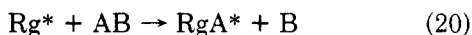
The latter process is the basis of operation for the rare-gas excimer laser.[184] Because of the large number of product channels available, a comprehensive description of the dynamics of metastable inert gas collisions has not been formulated. Nevertheless, considerable insight has been gained by focusing on the entrance channel.

The effect of reagent rare-gas spin–orbit states has been studied in processes 13, 14, 15, 19, and 20. The earliest studies involved the measurement of the total collisional removal rate for inert gas atoms in the metastable $^3P_0°$ and $^3P_2°$ states. Velazco, Kolts, and Setser[14] have provided a compilation of most of the available data on the bimolecular quenching rate constants for argon atoms in the $3p^54s$ configuration. In

many cases, the quenching rate constants are sizeable, comparable to or larger than the gas kinetic collision rate. For these quenchers, the differences between the different initial states are small, but the quenching cross section appears to increase with increasing reactant electronic energy. For reagents with small quenching rate constants, the rate is more variable. We mention in particular two reagents, Kr and CO, which illustrate opposite types of behavior. The Kr quenching rate constants for the $^3P_2°$ and $^3P_0°$ metastable states have been determined by Dreiling and Sadeghi[17] to be $k_2 = (4.90 \pm 0.20) \times 10^{-12}$ and $k_0 = (1.14 \pm 0.01) \times 10^{-13}$ cm^3 $molecule^{-1}$ s^{-1}, respectively. The ratio of the rate constants is in reasonable agreement with that determined by Golde and Poletti[122] but considerably greater than that reported by Velazco et al.[14] The large $^3P_2°$ quenching rate is explained by efficient near-resonant energy transfer to the $4p^55p$ states of Kr, from which emission is observed.[17,185] For CO, Golde and Poletti[122] find $k_0/k_2 = 8.1 \pm 1.5$, which agrees reasonably well with that calculated from the rate constants given by Velazco et al.[14] For this reagent, the major quenching channel is thought to be dissociation (eq 8);[122] a small energy barrier for the $^3P_2°$ reactant would account for its reduced rate constant. This opposite ordering of reactivity between Kr and CO has been utilized[60] for state selection of metastable argon atoms, as described in section III.C.

The effect of incident spin–orbit level on specific product channels has been investigated by monitoring the reaction products while selecting the spin–orbit state either optically (section III.B) or collisionally (section III.C). The excimer formation channel (eq 20) provides an illustration of the influence of inner-shell electrons in determining the course of a reaction. The production of the inert gas halide electronically excited ionic states from Rg* + RX reactants is believed to occur through an electron-jump mechanism involving a Rg^+RX^- intermediate;[183,186,187] this channel competes with direct energy transfer from the excited atom to the RX collision partner. The excimer products can be formed in three molecular states: $B(\Omega = 1/2)$ and $C(\Omega = 3/2)$, which correlate diabatically to the separated species $Rg^+(^2P_{3/2}°) + X^-$, and the $D(\Omega = 1/2)$ state, which dissociates to $Rg^+(^2P_{1/2}°) + X^-$. Four strong emission bands are expected in the radiative decay of these states to the mainly repulsive covalent states: B–X, B–A, C–A, and D–X.[188] For reactions of $Ar(^3P_2°)$ with a number of organic halides, the B–X continuum is the strongest feature, with the weaker B–A and C–A emission occurring to longer wavelengths.[60,76] It is estimated[76] that >95% of the excimer products are formed in the B and C states. By contrast, significant D–X emission is observed with $^3P_0°$ reactants;[60] the B to D state product ratio is estimated to be approximately 2.[76] While both the $^3P_2°$ and $^3P_0°$ states have an outer 4s electron, the angular momentum of the ionic core is $j = 3/2$ and 1/2, respectively. In the absence of core switching effects, $^3P_2°$ reagents would be expected to form $Rg^+(^2P_{1/2}°)X^-$ ionic products in the B and C states, as found.[60,76] Similarly, $^3P_0°$ reactants should yield D-state excimer products; the significant formation of the B state for $^3P_0°$ + RX reactions is attributed[76] to core switching effects at the crossings of the ionic surface with covalent surfaces correlating

to lower energy $^3P_1^\circ$ and $^3P_2^\circ$ states. Differences in the production rates of the various excited $np^4(n+1)s$ $^{2,4}P_J$ states of Cl and Br atoms produced by dissociative excitation (eq 19) have also been observed for Ar-$(^3P_{0,2}^\circ)$–halogen donor collisions.[60] Because of the nonstatistical distributions observed, this channel has been postulated as proceeding through predissociation of product RgX* halide. The variation of the excited halogen state populations is thus ascribed to differences in the formation rate of the excited RgX* states.

The excimer formation channel has also been compared for Kr and Xe $^3P_1^\circ$ and $^3P_2^\circ$ reactants.[117,187,189] The product emission spectra are fairly similar for the halide donors studied. The principal differences are an extension of the B–X spectrum to shorter wavelengths and evidence in the C–A system of greater C state product vibrational excitation for the $^3P_1^\circ$ reactant. The additional electronic energy of the $^3P_1^\circ$ vs. $^3P_2^\circ$ state can explain these differences. The excimer formation rate constants for the Xe $^3P_2^\circ$ and $^3P_1^\circ$ reactions have also been compared for several halide donors, and some variation in the ratio of these rate constants is found.[116,189] This reaction channel has also recently been studied for several of the higher excited radiating Xe(5p^{5}6p) states.[107] While the 5p^{5}6p total quenching rate constants are only somewhat larger than for the metastable 5p^{5}6s $^3P_2^\circ$ level (except for NF$_3$), the excimer product branching fractions are significantly enhanced, by a factor of $\sim$40 in the case of HCl.[107]

Spin–orbit effects have also been studied for several of the nonreactive decay pathways for metastable inert gas collisions. Optical pumping state selection has been employed to compare the rate of excitation transfer (eq 13) collisions of metastable Ar($^3P_0^\circ$ and $^3P_2^\circ$) with hydrogen atoms to yield excited H*($n = 2$). It is found that the higher energy $^3P_0^\circ$ state has a considerably lower rate constant for this channel than $^3P_2^\circ$: k_0/k_2 = 0.09 ± 0.025.[18] By consideration of Ω-state correlations between the separated atoms and excited ArH potentials,[190] this selectivity is explained[18] as arising from the access of the Ar($^3P_2^\circ$) + H entrance channel to the attractive B $^2\Pi$ and E $^2\Sigma^+$ ArH states, which can lead to H*($n = 2$) production by curve crossing with the B $^2\Pi$ and C $^2\Sigma^+$ states. By contrast, Ar($^3P_0^\circ$) + H correlates with a repulsive ArH $^4\Pi$ curve.

The $^3P_0^\circ$ and $^3P_2^\circ$ incident levels are observed to yield significant differences in the vibration–rotation state distribution of excited N$_2$(C $^3\Pi_u$) formed by excitation transfer in metastable argon–N$_2$ collisions.[16] While the vibrational distribution is somewhat hotter for the higher energy $^3P_0^\circ$ reagent, the relative rate coefficients cannot be explained by a golden-rule model.[16(b)] Resonance effects could be playing a role here since the $v' = 3$ level (which can only be excited by $^3P_0^\circ$, and not $^3P_2^\circ$, atoms) is greatly enhanced relative to $v' = 1$ or 2 at reduced temperatures. From high-resolution studies of the N$_2$ C $\rightarrow$ B emission,[16(a),182] the spin and Λ-doublet levels have been found to be unequally populated, giving rise to an even–odd N alternation in the rotational populations. This preferential population has been explained in part as implying the dominance of planar ArNN collisions.[16(a)] These intensity alternations are also found to depend on the identity of the incident Ar* level. To account for this dependence, additional dynamical constraints including

the preferential population of Λ-doublets whose electronic distribution is symmetric with respect to the plane of rotation must be introduced.

Considerable attention has been paid to the ionization channels for the reaction of metastable rare gas atoms with a variety of species. Golde and Ho[123] measured the branching fractions f_{ion} for chemi-ion formation for Ar($^3P_2^\circ$ and $^3P_0^\circ$)—halogen donor interactions. In some reactions, significant differences in f_{ion} between the two reagent levels are observed but can be explained simply by energetic arguments; it appears that f_{ion} increases sharply as the reagent electronic energy becomes larger than the threshold for Penning ionization (eq 14). The velocity dependence of the total ionization cross section has also been measured for collisions of state-selected Ne($^3P_2^\circ$ and $^3P_0^\circ$) atoms with the heavier inert gases and N$_2$.[23] The higher energy $^3P_0^\circ$ state is again found to have larger ionization cross sections, with the ratio of $^3P_0^\circ$ to $^3P_2^\circ$ cross sections decreasing somewhat with increasing velocity. This behavior can be explained by differences in the real part of the repulsive potential.

The translational energy distribution of electrons released in Penning and associative ionization (eq 14 and 15, respectively) has been investigated for state-selected metastable Ne($^3P_2^\circ$ and $^3P_0^\circ$) and higher Ne-(2p^{5}3p) states by Hotop and co-workers.[19–21,25,26] As with the excitation transfer discussed above for Ar* + H, the total ionization cross section for Ne* + H,D collisions is found[20] to be much smaller for $^3P_0^\circ$ than $^3P_2^\circ$ reagent; the difference is likewise explained as due to the correlation of these states with repulsive and attractive molecular potentials, respectively. Consistent with this conclusion is the observation of a very broad electron energy distribution for Ne($^3P_2^\circ$) + H,D but a narrow one for $^3P_0^\circ$. Similar observations have been reported for ionizing collisions with alkali atoms.[25] For Penning ionizing collisions of Ne($^3P_{2,0}^\circ$) with the heavier inert gases Rg, analysis of the electron energy distribution shows a nonstatistical population of the fine-structure levels of the product Rg$^+$($^2P_{3/2,1/2}^\circ$) ions.[19] This has been explained[22] as arising from the interference of two transition amplitudes, which correspond to the transfer of a σ or π electron, respectively, on the Rg atom into the 2pσ or 2pπ hole, respectively, on the Ne atom, with ejection of the Ne 3s electron; $\sigma \rightarrow \sigma$ transfer is concluded to be dominant. A similar interpretation has been given for the experimental observations on collisions of highly excited Ne(2p^{5}3p J = 1,2,3) atoms with Ar and Kr.[21,98] A preferential population of excited Ca$^+$ 4 $^2P_{3/2}^\circ$ vs. 4 $^2P_{1/2}^\circ$ ions is also found in Penning ionizing collisions of Ar($^3P_{0,2}^\circ$) with Ca.[191]

2. Ions

Spin–orbit effects have also been observed in ion-molecule chemical reactions and charge transfer collisions. The ion-molecule reaction Rg$^+$ + H$_2$ $\rightarrow$ RgH$^+$ + H has the same valence electronic configuration as the F + H$_2$ reaction discussed in section IVA. However, in the present case, an additional process, namely charge transfer to form Rg + H$_2^+$, is also allowed, at least for Ar$^+$. Tanaka et al.[27] have utilized the TESICO technique to study the spin–orbit dependence of both the chemical reaction and charge transfer channels in Ar$^+$ + H$_2$ collisions. In both cases, the cross section for the $^2P_{1/2}^\circ$ initial state is found to be larger, with a ratio

TABLE IV. Alkaline Earth Halide Chemiluminescence Cross Sections for M* + RX Reactions

reaction	MX* state	σ_{chem} $(\text{Å}^2)^a$	$\sigma_J/\sigma_{chem}{}^b$		
			$J = 0$	1	2
$Ca(^3P^\circ) + Cl_2{}^c$	A	36.8 ± 5.2	0.02 ± 0.11	0.47 ± 0.13	1.35 ± 0.23
	B		0.11 ± 0.12	0.38 ± 0.12	1.35 ± 0.23
$Ca(^3P^\circ) + CH_3Br^c$	A	0.28 ± 0.09	0.00 ± 0.17	0.47 ± 0.18	1.39 ± 0.27
$Ca(^3P^\circ) + CH_3I^d$	A/B^e	1.34 ± 0.24	0.23 ± 0.13	0.10 ± 0.11	1.43 ± 0.26
$Ca(^3P^\circ) + CH_2Br_2{}^c$	A	1.7 ± 0.3	0.05 ± 0.11	0.28 ± 0.12	1.37 ± 0.24
$Ca(^3P^\circ) + CH_2I_2{}^d$	A/B^e	9.52 ± 1.26	0.01 ± 0.11	0.33 ± 0.12	1.41 ± 0.25
$Ca(^3P^\circ) + CH_2CHCH_2Br^c$	A	2.6 ± 0.4	0.16 ± 0.12	0.29 ± 0.12	1.38 ± 0.24
$Ca(^3P^\circ) + C_6H_5CH_2Br^c$	A	1.00 ± 0.14	0.25 ± 0.14	0.88 ± 0.21	1.22 ± 0.21
			σ_0/σ_2		
$Sr(^3P^\circ) + Cl_2{}^f$	A	g	0.14 ± 0.17		
	B		0.22 ± 0.19		
$Sr(^3P^\circ) + Br_2{}^f$	A	g	0.17 ± 0.17		
	B		0.18 ± 0.17		
$Sr(^3P^\circ) + CH_2Br_2{}^f$	A	g	0.19 ± 0.18		
$Sr(^3P^\circ) + CH_2I_2{}^f$	A/B^e	g	0.12 ± 0.18		

^{a} σ_{chem} pertains to the production of the MX A and B states. ^{b}Defined in eq 8. ^{c}Reference 72. ^{d}Reference 73. ^{e}A–X and B–X band systems overlapped. ^{f}Reference 74. ^{g}Not measured.

for $^2P_{1/2}{}^\circ$ to $^2P_{3/2}{}^\circ$ reactants of 1.5 and 7, respectively, independent of initial collision energy. This confirms the results of an early photoionization study of the reaction by Chupka and Russell.[192] A similar ratio (1.3) was found for the atom transfer reaction with $Ar^+ + D_2$, while no spin–orbit dependence was observed for the corresponding charge-transfer channel.[27]

The observed higher reactivity of the Ar^+ $^2P_{1/2}{}^\circ$ state is contrary to that for the $F + H_2$ reaction, as discussed in section IVA. This has been explained[27] by the mediation of the charge-transfer potential energy surface in the ion–molecule reaction: The reactant $Ar^+ + H_2$ surface correlates to $Ar^+ + H + H$ fragments, while both $Ar + H_2{}^+$ and $ArH^+ + H$ correlate to $Ar + H^+ + H$.[193,194] This implies a nonadiabatic process is required for reaction. While the reactant $Ar^+(^2P_{1/2}{}^\circ) + H_2(v = 0)$ level is nearly isoenergetic with $Ar + H_2{}^+(v = 2)$, the spin–orbit dependence in the nonresonant $Ar^+ + D_2$ reaction and the identical translational dependence for the two reactant spin–orbit states argues against vibronic resonance effects. The opposite ordering of reactivity has been found[33] for the $Kr^+ + H_2$ atom transfer reaction: $k(^2P_{1/2}{}^\circ)/k(^2P_{3/2}{}^\circ) = 0.6 \pm 0.2$.

Spin–orbit effects have also been found in charge-transfer collisions. Liao et al.[31] have observed in a crossed-beam photoionization apparatus that the $^2P_{1/2}{}^\circ$ state has a considerably smaller cross section than $^2P_{3/2}{}^\circ$ in $Ar^+ + N_2$ collisions. They found $\sigma(^2P_{1/2}{}^\circ)/\sigma(^2P_{3/2}{}^\circ)$ reaches a minimum value of 0.2 at E_{lab} near 10 eV but increases somewhat at higher and lower energies. This is significantly smaller than the ratio (approximately 0.6) observed earlier by Kato et al.[28] The higher value has been ascribed to partial collisional equilibration effects in the photoionization chamber.[30,195] A similar large spin–orbit effect was seen[28] in $Ar^+ + CO$ charge transfer collisions; the $^2P_{1/2}{}^\circ$ to $^2P_{3/2}{}^\circ$ cross section ratio was determined to be ~ 0.15. A semiclassical calculation[196] of the charge-transfer cross section for $Ar^+ + N_2$ also finds a smaller reactivity for $^2P_{1/2}{}^\circ$ vs. $^2P_{3/2}{}^\circ$.

The cross section for the $^2P_{1/2}{}^\circ$ state relative to that for $^2P_{3/2}{}^\circ$ is found to be slightly less than unity for moderate energies for symmetric charge exchange in argon, krypton, and xenon;[30,32,197] however, this ratio approaches unity at low- and high-collision energies. The broad minimum in the ratio has been observed in impact parameter calculations on the Kr and Xe sys-

tems[198] and occurs in the energy region where the kinetic energy is comparable to the spin–orbit splitting.

C. Metastable Alkaline Earth Metal Atoms

In our laboratory, the optical pumping-state selection technique (section III.B) has been utilized to study spin–orbit effects in reactions of the lowest atomic triplet state ($^3P^\circ$ for Ca and Sr, ^3D for Ba) with various halogen compounds.[70–75] For most of these reactants, several exit channels are energetically accessible, including a reaction to form ground-state products,
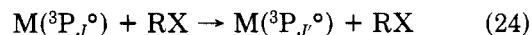
$$M^* + RX \rightarrow MX(X) + R \qquad (21)$$
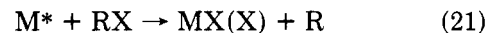
or electronically excited chemiluminescent products,

$$M^* + RX \rightarrow MX^*(A,B,C) + R \qquad (22)$$

as well as chemi-ionization,

$$M^* + RX \rightarrow MX^+ + R^- \qquad (23)$$
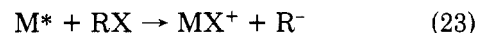
In addition, several nonreactive decay pathways are available: intramultiplet mixing, e.g.,

$$M(^3P_J{}^\circ) + RX \rightarrow M(^3P_{J'}{}^\circ) + RX \qquad (24)$$

and collisional quenching,

$$M^* + RX \rightarrow M(^1S) + RX \qquad (25)$$
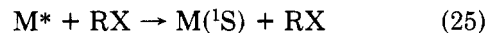
The latter is not expected to be significant for halogen donors.

The dependence of the chemiluminescence cross section (reaction 22) on the incident spin–orbit level has been determined for a number of diatomic and polyatomic halogen donors. Table IV presents these results, obtained by the use of eq 6–8, along with the absolute chemiluminescence cross sections, σ_{chem}, which were measured with an unpumped spin–orbit distribution (see eq 6) by comparing reactant and product emission intensities.[199,200] Because of the congestion in the alkaline earth halide spectra, the expected high degree of product internal excitation, and the low spectral resolution in these experiments, these data apply to total formation rates for the electronic states and not to production of individual vibrational levels. The Ca, Sr, and Ba atoms possess a second optically metastable level (^1D) whose electronic energy is somewhat greater than the metastable triplet. In some reactions, the ^1D component in the reagent atomic beam contributes

significantly to the observed product signal. The ^1D contribution has been taken into account for Ca and Ba by observing the change in the product signal when the ^1D level is optically depleted.[72,73,75]

With the sole exception of $Ca(^3P°) + SF_6$,[73] all the reactions studied exhibit a significant spin–orbit dependence in reaction 22. The highest energy spin–orbit level ($J = 2$ for $^3P°$, $J = 3$ for ^3D) is found to have the largest cross section, and lower J levels show successively smaller values. The $J = 2$ cross sections are roughly 5 to 10 times larger than that for $J = 0$ for Ca and Sr $^3P°$; the differences between Ba $^3D_3$ and $^3D_1$ are comparable.[75]

For several Ca and Sr reactions, it has been possible to study the ground-state product (reaction 21) by laser fluorescence detection.[71,74] An opposite ordering of reactivity was observed for this channel, with the $J = 0$ level exhibiting the largest cross section. The ratio σ_0/σ_2 of the cross section for reaction 21 for the $J = 0$ and 2 incident states was found to be 1.93 ± 0.36 and 3.08 ± 0.54 for $Sr(^3P°) + CH_2Br_2$ and HBr, respectively;[74] a similar ratio was found for $Ca(^3P°) + Cl_2$,[71] although the experimental uncertainty was large because of the background signal from the $Ca(^1S)$ reaction. Much smaller spin–orbit effects were observed for the chemi-ionization channel (reaction 23) for the $Ca(^3P°) + Cl_2$, Br_2 reactions.[70]

In spite of the large cross sections expected for these chemical reactions, nonreactive intramultiplet mixing (reaction 24) was also observed. When the Ca $^3P_1°$ level was optically depleted, the $^3P_1° \rightarrow {}^1S$ emission signal was found[70,72,73] to increase initially with increasing target gas density, indicating collisional transfer into $^3P_1°$ from the nonradiating $^3P_{0,2}°$ states. A simple kinetic model was used to estimate cross sections for this process. In some reactions, these were found to be sizeable.

These reactions proceed by charge transfer to form the ionic alkaline earth monohalide product; because of their large positive electron affinities,[201] charge transfer occurs at relatively large separations for Cl_2[202] and Br_2. At least for the diatomic halogens, broadside C_{2v} approach is the favored orientation for reaction.[70,105,202,203] As the reagents approach but before charge transfer, several electrostatic surfaces corresponding to different orientations of the metal valence p (or d) electron will arise. In C_{2v} geometry, only for the $^3B_2$ surface is charge transfer to the lowest ionic surface symmetry allowed.[70,105,203] Figure 5 shows for $^3P°$ reactants that there is good overlap of the metal p orbital and the lowest unoccupied σ_u^* orbital of the halogen molecule only for this symmetry species.

In fact, there are three interactions of importance in understanding spin–orbit effects in chemical reactions, as in nonreactive collisional intramultiplet mixing:[36,204] spin–orbit coupling, electrostatic interactions, and nuclear rotation. For the separated species, the former is dominant, and the vector sum of $\bar{L}$ and $\bar{S}$ of the metal atom are strongly coupled to form $\bar{J}$ but are weakly coupled to the interparticle axis, defining a Hund's case (e) representation. At smaller separations, the electrostatic interactions described above become important, and a case (a) representation applies. It is not possible to diagonalize the complete Hamiltonian[36,204] with a transformation independent of the interparticle
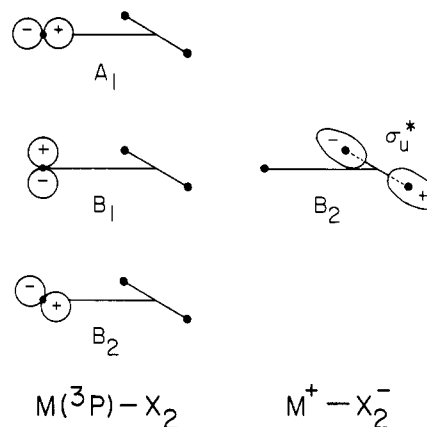
Figure 5. Comparison of the p orbital orientation for the $M(^3P°)$ – X_2 covalent surfaces in C_{2v} symmetry with that of the σ_u^* orbital of X_2^- for the lowest $M^+ - X_2^-$ ionic surface.

separation. Thus, an incident spin–orbit level J will generate flux on more than one electrostatic surface. This nonadiabatic mixing is the origin of collisional fine-structure transitions in nonreactive collisions.[35,36] Qualitatively, spin–orbit effects in chemical reactions can be explained as arising from differences in the evolution of the asymptotic spin–orbit states onto the covalent electrostatic surfaces, from which charge transfer occurs with differing probabilities.

Alexander[205] has implemented a pseudo-quenching fully quantum mechanical model to test these ideas for $Ca(^3P°)-Cl_2$ collisions. We note that such a model is not restricted to the calcium atom but can also be used to understand spin–orbit effects involving other types of atoms. In Alexander's model, reaction is simulated by an atom–atom collision in which the diabatic covalent curves correlating to $Ca(^3P°)$ are crossed at long range by an attractive potential to mimic the ionic-covalent crossing. The latter is allowed to couple directly with only one covalent curve. To mimic reaction, the ionic curve is coupled at smaller separations to a repulsive curve correlating to a lower energy asymptote. Significant differences in the magnitudes of the pseudoquenching cross sections vs. incident spin–orbit level were found; the cross sections were extremely sensitive to the strength of the ionic–covalent coupling. In view of the expected importance of nonadiabatic coupling for an atom such as $Ca(^3P°)$ with relatively small spin–orbit splittings, it is interesting to note that simple adiabatic correlation arguments can qualitatively explain the ordering of reactivity. In all cases, independent of which covalent curve was directly coupled to the ionic curve and even the assumed sign of the Ca spin–orbit constant A (see eq 1), the pseudoquenching cross section was largest for the lowest energy spin–orbit state.

The calculations of Alexander[205] provide an explanation for the ordering of reactivity in the ground-state channel (eq 21). The chemiluminescence channel (eq 22) requires access to excited ionic surfaces, which can be reached by diabatic traversal of the outermost ionic–covalent crossing.[70,71,203] The larger $^3P_2°$ chemiluminescence cross sections can be explained by the fact that flux from $^3P_2°$ reactants is least efficiently removed at this outermost crossing.[70,71]

Symmetry restrictions to charge transfer might be expected to be less important for polyatomic reactants.

TABLE V. Chemiluminescence and Total Cross Sections for Metastable $Hg(^3P_J^\circ)$–Halogen Donor Collisions

reactant	σ_{chem} (Å^2)		σ_{tot} (Å^2)	
	$J = 2$	$J = 0$	$J = 1$	$J = 0$
Cl_2	90 ± 25^a	0.26 ± 0.1^b	91 ± 5^c	28^b
Br_2	160 ± 50^e	$3^{+3}_{-2}{}^f$	100^g	44^h
	186^d			
F_2	222^d			
CCl_4	34 ± 10^a			
	21.5^i			
$CHCl_3$	7.9 ± 1.8^a			
	6.2^i			

^{a} Reference 129. ^{b} Reference 206. ^{c} Reference 207. ^{d} Reference 61. ^{e} Unpublished results of H. F. Krause and S. Datz reported in ref 127. ^{f} Reference 127. ^{g} Unpublished results of C. B. Roxlo reported in ref 208. ^{h} Reference 209. ^{i} Reference 208.

It is thus surprising that the spin–orbit dependence is essentially the same for these more complicated species as for the diatomic halogens.[70,72-74] However, symmetry restrictions can be invoked[73] for the methyl halide reactions, for which collinear M–X–C approach is expected to be most favorable for reaction. It might also be expected that larger spin–orbit effects will be manifest for the heavier alkaline earth atoms since nonadiabatic effects should be smaller for the latter due to the larger asymptotic spin–orbit splitting (see Table II). Observation[70,72] of intramultiplet mixing (eq 24) shows that such mixing occurs in $Ca(^3P^\circ)$ collisions. However, within the relatively large experimental errors, no significant difference in the spin-orbit dependence between Ca and Sr is apparent in Table IV. It may be that the transition from cases (a) to (e) occurs at separations larger than the charge-transfer radius for all the reactions studied.

D. Metastable Mercury and Cadmium Atoms

Reactions of metastable $Hg(^3P^\circ)$ atoms with a variety of halogenated compounds have been found to produce intense HgX B $^2\Sigma^+$ – X $^2\Sigma^+$ chemiluminescence, in analogy to reaction 22 discussed in Section III.C. The principal differences between these two classes of reactions are the bound-free nature of the HgX* emission because of the small ground-state dissociation energy and the very large Hg spin–orbit splittings (see Table II). The weak ground-state binding energy makes these reactions similar to the corresponding metastable inert gas reactions. The reactions of metastable mercury, alkaline earth, and inert gas atoms all proceed by charge transfer to form ionic products.

Chemiluminescence cross sections as a function of $Hg(^3P^\circ)$ spin–orbit level J have been measured in several molecular beam[127,129] and flowing afterglow[61,208] experiments. These are reported in Table V, along with cross sections for collisional removal by all pathways for $Hg(^3P_0^\circ)$ and $^3P_1^\circ)$ + Cl_2 and Br_2.[206,207,209] It can be seen that there is a striking spin–orbit dependence in the Cl_2 and Br_2 reactions, for which data on both the $J = 0$ and 2 levels are available. Moreover, σ_{chem} for $J = 2$ is comparable to σ_{tot} for the other spin–orbit levels and to the total reaction cross sections of comparable alkali atom reactions.[201,208] Thus, the branching fraction f_{chem} for the chemiluminescence channel must be close to unity for $^3P_2^\circ$ reactants, at least for the diatomic halogen reactions. This contrasts with the corresponding alkaline earth reactions, where f_{chem} is typi-

cally 30% or less.[70,72,200,203] The general discussion given in the previous section for alkaline earth atom reactions can be applied to $Hg(^3P^\circ)$ reactions. However, the very large $Hg(^3P^\circ)$ spin–orbit splitting implies that nonadiabatic mixing in the entrance channel will be negligible, and the higher energy $^3P_2^\circ$ reactant can efficiently reach excited potential energy surfaces correlating with the chemiluminescent HgX(B) product, while the lower spin–orbit states yield only nonemitting products. Dreiling and Setser[208] have given a detailed comparison, with similar arguments about the spin–orbit selectivity, of the $Hg(^3P^\circ)$ reactions with the corresponding alkali and metastable alkaline earth and inert gas reactions.

Callear and McGurk[210] have determined the absolute yield of HgH and/or HgD from the reactions of $Hg(^3P_0^\circ$ and $^3P_1^\circ)$ with H_2 and its isotopic analogues. Only small differences were observed between the corresponding $^3P_0^\circ$ and $^3P_1^\circ$ reactions.

In several studies of the nonreactive electronic quenching of $Cd(^1P^\circ)$, Breckenridge and co-workers[35] have determined the spin–orbit state distribution of $Cd(^3P_J^\circ)$ products by a pump and probe technique. For some collision partners, the J state distribution is skewed away from a statistical ratio toward preferential $J = 2$ formation.

E. Germanium, Tin, and Lead

The total collisional removal rates for the ^3P_J spin–orbit levels of Ge, Sn, and Pb have been measured by both time-resolved and flow techniques for a number of collision partners. Table VI summarizes the available data for those species where chemical reaction is energetically allowed. Similar data have been obtained for the lighter elements of this group, but for these atoms rapid collisional equilibration of the spin–orbit levels prevented observation of spin–orbit-dependent effects.[59,223-225]

Inspection of Table VI shows some dramatic spin–orbit dependences in the collisional removal rates, particularly for the Sn, Pb + N_2O reactions, for which the rates fall in the order $J = 0 < J = 1 < J = 2$. With the exception of Sn + CO_2, only relatively small differences in the rates are seen in other reactions. If we assume for Sn, Pb + N_2O that nonreactive quenching is unimportant for the excited spin-or' it levels, the increase in rate with increasing J could ⸱e simply due to an increased reaction exothermicity for $J = 1$ and 2; however, these reactions are already substantially exothermic for the $J = 0$ level.

Adiabatic correlation diagrams in the strong spin–orbit coupling limit have been used to rationalize the reactivity of electronically excited heavy metal atoms.[12,53] Figure 6 presents such a diagram for the Sn + N_2O reaction;[213] similar diagrams can be drawn for the corresponding Ge and Pb reactions. This reaction is notable because of the very high branching ratio (photon yield approximately 50%[58]) found for the production of chemiluminescent SnO molecules (principally a $^3\Sigma^+$ and b $^3\Pi$). A significant activation energy ($\sim$4 kcal/mole) and relatively small preexponential factor were found from the temperature dependence of the $Sn(^3P_0)$ + N_2O reaction rate.[216,217] These observations may be reconciled if it is assumed[58] that it is the $^3P_1$ state, and not $^3P_0$ state, that reacts and yields SnO*. Indeed, the (J,Ω) coupling correlation diagram in Figure

TABLE VI. Bimolecular Rate Constants (in cm³ molecule⁻¹ s⁻¹) for the Total Collisional Removal Rate of Group IVA (14) ³P_J Atoms (T = 295–300 K Unless Otherwise Stated)

reactant	$\Delta H_0^{\circ\,a}$ (kcal/mole)	k : $J = 0$	1	2
		Ge(4p² ³P)		
N₂O	−118	$(5.8 \pm 0.8) \times 10^{-12\,b}$ $(9.9 \pm 0.9) \times 10^{-12\,c}$ $(5.7 \pm 0.6) \times 10^{-12\,d}$ $(1.2 \pm 0.6) \times 10^{-12}$ (350 K)^e $(4.2 \pm 1) \times 10^{-12}$ (350 K)^{f,g}	$(5.3 \pm 0.1) \times 10^{-12\,b}$ $(3.6 \pm 0.6) \times 10^{-12\,d}$ $(1.3 \pm 0.6) \times 10^{-12}$ (350 K)^e $(8.4 \pm 3) \times 10^{-12}$ (350 K)^{f,g}	$(9.5 \pm 0.7) \times 10^{-12\,b}$ $(6.9 \pm 2) \times 10^{-12}$ (350 K)^{f,g}
O₂	−38	$(1.2 \pm 0.1) \times 10^{-10\,h}$ $(2.5 \pm 0.1) \times 10^{-10\,c}$	$(1.3 \pm 0.1) \times 10^{-10\,h}$ $(2.4 \pm 1.2) \times 10^{-11}$ (350 K)^e	$(1.5 \pm 0.3) \times 10^{-10\,h}$
CO₂	−31	$(6.0 \pm 0.5) \times 10^{-12\,b}$	$(3.6 \pm 0.1) \times 10^{-12\,b}$	$(8.0 \pm 0.2) \times 10^{-12\,b}$
NO	−6	$(3.8 \pm 0.6) \times 10^{-12\,h}$	$(2.5 \pm 0.2) \times 10^{-12\,h}$ $(1.0 \pm 0.5) \times 10^{-12}$ (350 K)^e	$(2.1 \pm 0.2) \times 10^{-12\,h}$
		Sn(5p² ³P)		
N₂O	−88	$(6.4 \pm 2.4) \times 10^{-16\,f,i}$ $6.2 \times 10^{-15\,f,j}$ $4.7 \times 10^{-16\,g}$	$(1.1 \pm 0.1) \times 10^{-12\,i}$ 9×10^{-13} (315 K)^k 1.1×10^{-12} (500 K)^l	$(3.5 \pm 0.7) \times 10^{-11\,i}$
O₂	−9	$(3.49 \pm 0.4) \times 10^{-11\,m}$ $(2.1 \pm 0.1) \times 10^{-11\,j}$ 2×10^{-11} (315 K)^k $(1.05 \pm 0.08) \times 10^{-11\,c}$	$(8.20 \pm 0.5) \times 10^{-11\,m}$ 2×10^{-10} (330 K)^k	$(4.9 \pm 0.3) \times 10^{-11\,m}$
CO₂	−1	$\leqslant 2 \times 10^{-17}$ (573 K)^j	$(3.2 \pm 0.2) \times 10^{-13\,n}$	$(6.2 \pm 0.6) \times 10^{-12\,n}$
		Pb(6p² ³P)		
N₂O	−50	$<1.8 \times 10^{-15\,o}$	$(2.8 \pm 1.0) \times 10^{-14\,p}$	$(4 \pm 1) \times 10^{-13\,p}$
O₂	+29		$(7.0 \pm 5.0) \times 10^{-12\,p}$ $4.5 \times 10^{-11\,q}$	$(4.0 \pm 1.0) \times 10^{-11\,p}$ $4.6 \times 10^{-11\,q}$

^{a} Exothermicity for ³P₀ reactants (dissociation energies taken from ref 211); values for other J levels can be obtained with the help of Table I. ^{b} Reference 212. ^{c} Reference 213. ^{d} Reference 214. ^{e} Reference 59. ^{f} Extrapolated to given temperature using the quoted Arrhenius parameters. ^{g} A. Fontijn, private communication cited in ref 59. ^{h} Reference 215. ^{i} Reference 216. ^{j} Reference 217. ^{k} Reference 58. ^{l} Reference 218. ^{m} Reference 219. ^{n} Reference 227. ^{o} Reference 220. ^{p} Reference 221. ^{q} Reference 222.

TABLE VII. Bimolecular Rate Constants (in cm³ Molecule⁻¹ s⁻¹ at 300 K) for the Total Collisional Removal Rate of Group VA (15) ²D_J° Atoms

reactant	Sb^a : $J = 3/2$	5/2	Bi^b : $J = 3/2$	5/2
H₂	$(6.6 \pm 0.2) \times 10^{-12}$	$(2.5 \pm 0.3) \times 10^{-12}$	$(7.9 \pm 0.8) \times 10^{-14}$	$(5.6 \pm 0.5) \times 10^{-12}$
O₂	$(1.7 \pm 0.1) \times 10^{-11}$	$(1.8 \pm 0.2) \times 10^{-11}$		$(8.1 \pm 0.6) \times 10^{-12}$
CO₂	$(2.1 \pm 0.5) \times 10^{-13}$	$<1 \times 10^{-13}$	$<4 \times 10^{-15}$	$(2.1 \pm 0.1) \times 10^{-13}$
N₂O			$(1.9 \pm 0.2) \times 10^{-14}$	$(3.8 \pm 0.2) \times 10^{-14}$

^{a} Reference 229. ^{b} Reference 230.

6 provides a rationalization for the reactivity of the ³P₁ level. This argument has been criticized[213] because it offers no explanation for the low reactivity of ³P₀ to form ground-state SnO. Alternatively, the 4 kcal/mol activation barrier has been ascribed[216] to an avoided crossing between states correlating diabatically with Sn + N₂O(X ¹Σ⁺) and Sn + N₂O(³Σ⁺) because the N₂O molecule adiabatically dissociates to form excited O(¹D), rather than ground-state O(³P) atoms.

Adiabatic correlation diagrams in (J,Ω) coupling have also been used to explain the differences in collisional removal rates observed for other reactant partners.[213,215,219,226,227] For example, the slightly larger rate seen[219] for Sn(³P₁) + O₂ vs. Sn(³P₂) + O₂ was rationalized by the fact that the ³P₁ reactant is adiabatically connected to exothermic SnO(X ¹Σ⁺) + O products, while the ³P₂ reactant correlates with energetically inaccessible excited products. However, a similar ordering of removal rates was not observed for Pb + O₂, for which an analogous correlation diagram applies. Here reaction to form ground-state PbO products is endothermic, at least for the ³P₀,₁ levels. In this case, the collisional decay is further complicated by what appears to be rapid electronic equilibration by E–E transfer:[228]

$$\text{Pb}(^3P_1) + O_2(X\ ^3\Sigma_g^-) \rightleftarrows \text{Pb}(^3P_0) + O_2(a^1\Delta_g) \qquad (26)$$
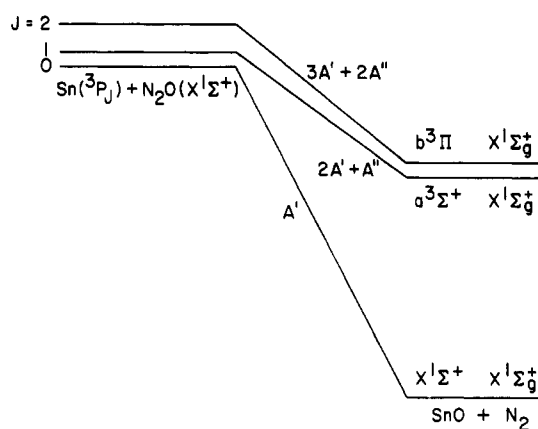
Figure 6. Adiabatic correlation diagram in the strong spin–orbit limit for Sn + N₂O → SnO + N₂.

By contrast, the Ge + O₂ removal rates are nearly equal for the three ³P_J spin–orbit levels;[215] this suggests there are limitations on the general utility of arguments based on correlation diagrams.

F. Other Metal Atoms

Some differences in the total collisional removal rates vs. incident spin–orbit level have been observed in the

quenching of the metastable $^2D^\circ$ manifold of Sb and Bi.[229,230] Results for reagents for which chemical reaction is possible are listed in Table VII. For the lighter As atom, the spin–orbit levels of the metastable $^2D^\circ$ and $^2P^\circ$ levels were found to maintain a Boltzmann equilibrium in similar experiments.[231] With Sb and Bi, H_2 and CO_2 quenching, either by nonreactive or reactive processes, requires a nonadiabatic process, as well as for Bi + O_2.[230] For Sb + O_2, adiabatic reaction channels are available for both spin–orbit levels. The slow removal rates for N_2O are somewhat surprising in view of the availability of adiabatic reaction pathways;[230] however, significant activation barriers are often found for reactions involving N_2O.[216,217,232]

Collisional removal rate constants have also been measured for the ground 6 $^2P_{1/2}^\circ$ and excited 6 $^2P_{3/2}^\circ$ spin–orbit levels of thallium.[233-235] For I_2, the excited state is found[233] to have only a slightly larger thermally averaged cross section: $\sigma_{3/2} = 159$ Å^2 vs. $\sigma_{1/2} = 105$ Å^2, with a $\sim15\%$ experimental error. It is interesting to note that while the ground state is removed by chemical reaction, the excited state undergoes almost exclusively nonreactive electronic deexcitation.

V. Acknowledgments

Note Added in Proof. Weister and Siska[237] have recently investigated metastable $Ne(^3P_{0,2}^\circ)$ + Ar ionizing collisions with optical pumping-state selection in a crossed-beam configuration and find a significant dependence of the fraction of association ionization (eq 15) on initial Ne spin–orbit state. By utilizing selective collisional relaxation of metastable $Hg(^3P_2^\circ)$ by N_2 (see sections III.C and IV.D), Zhang, Oba, and Setser[238] have been able to isolate the HgX* chemiluminescence from reaction of $Hg(^3P_0^\circ)$ with a number of halogen-containing reactants.

VI. References

(1) Levine, R. D.; Bernstein, R. B. *Molecular Reaction Dynamics*; Oxford University: New York, 1974.
(2) Smith, I. W. M. *Kinetics and Dynamics of Elementary Gas Reactions*; Butterworths: London/Boston, 1980.
(3) Bernstein, R. B. *Chemical Dynamics Via Molecular Beam and Laser Techniques*; Oxford University Press: New York, 1982.
(4) Levy, M. R. *Prog. React. Kinet.* 1979, 10, 1.
(5) Smith, I. W. M. In *Physical Chemistry of Fast Reactions*; Smith, I. W. M., Ed.; Plenum: New York, 1980; Vol. 2, p 1.
(6) Kneba, M.; Wolfrum, J. *Ann. Rev. Phys. Chem.* 1980, 31, 47.
(7) Holmes, B. E.; Setser, D. W. In *Physical Chemistry of Fast Reactions*; Smith, I. W. M., Ed.; Plenum: New York, 1980; Vol. 2, p 83.
(8) Polanyi, J. C.; Schreiber, J. L. In *Physical Chemistry, An Advanced Treatise*; Jost, W., Ed.; Academic: New York, 1974; Vol. VIA, p 383.
(9) Kuntz, P. J. In *Modern Theoretical Chemistry*; Miller, W. H., Ed.; Plenum: New York, 1975; Part B, Chapter 2.
(10) Henderson, D., Ed. *Theoretical Chemistry. Theory of Scattering: Papers in Honor of Henry Eyring*; Academic: New York, 1981; Vols. 6A, B.
(11) Leone, S. R. *Ann. Rev. Phys. Chem.* 1984, 35, 109.
(12) Husain, D. *Ber. Bunsenges. Physik. Chem.* 1977, 81, 168.
(13) Piper, L. G.; Setser, D. W.; Clyne, M. A. A. *J. Chem. Phys.* 1975, 63, 5018.
(14) Velazco, J. E.; Kolts, J. H.; Setser, D. W. *J. Chem. Phys.* 1978, 69, 4357.
(15) Loeb, D. W.; Chen, M.-C.; Firestone, R. F. *J. Chem. Phys.* 1981, 74, 3270.
(16) (a) Derouard, J.; Nguyen, T. D.; Sadeghi, N. *J. Chem. Phys.* 1980, 72, 6698. (b) Nguyen, T. D.; Sadeghi, N. *Chem. Phys.* 1983, 79, 41.
(17) Dreiling, T. D.; Sadeghi, N. *J. Phys. (Paris)* 1983, 44, 1007.
(18) Sadeghi, N.; Setser, D. W. *Chem. Phys.* 1985, 95, 305.
(19) Hotop, H.; Lorenzen, J.; Zastrow, A. *J. Electron. Spectrosc. Relat. Phenom.* 1981, 23, 347.
(20) Lorenzen, J.; Morgner, H.; Bussert, W.; Ruf, M.-W.; Hotop, H. *Z. Phys. A* 1983, 310, 141.
(21) Bussert, W.; Bregel, T.; Ganz, J.; Harth, K.; Siegel, A.; Ruf, M.-W.; Hotop, H. *J. Phys. (Paris)* 1985, 46, C1–199.
(22) Morgner, H. *J. Phys. B* 1985, 18, 251.
(23) Verheijen, M. J.; Beijerinck, H. C. W. *Chem. Phys.* 1986, 102, 255.
(24) Bruno, J. B.; Krenos, J. *J. Chem. Phys.* 1983, 78, 2800.
(25) Lorenzen, J.; Hotop, H.; Ruf, M.-W., submitted for publication in *Z. Phys. D.*
(26) Lorenzen, J.; Hotop, H.; Ruf, M.-W.; Morgner, H. *Z. Phys. A* 1980, 297, 19.
(27) Tanaka, K.; Durup, J.; Kato, T.; Koyano, I. *J. Chem. Phys.* 1981, 74, 5561.
(28) Kato, T.; Tanaka, K.; Koyano, I. *J. Chem. Phys.* 1982, 77, 337.
(29) Tiernan, T. O.; Lifshitz, C. *Adv. Chem. Phys.* 1981, 45, 81.
(30) Liao, C.-L.; Liao, C.-X.; Ng, C. Y. *J. Chem. Phys.* 1985, 82, 5489.
(31) Liao, C.-L.; Xu, R.; Ng, C. Y. *J. Chem. Phys.* 1986, 84, 1948.
(32) Campbell, F. M.; Browning, R.; Latimer, C. J. *J. Phys. B* 1981, 14, 1183.
(33) Smith, R. D.; Smith, D. L.; Futrell, J. H. *Chem. Phys. Lett.* 1975, 32, 513.
(34) Friedrich, B.; Vancura, J.; Sadilek, M.; Herman, Z. *Chem. Phys. Lett.* 1985, 120, 243.
(35) Breckenridge, W. H.; Kim Malmin, O. *Chem. Phys. Lett.* 1979, 68, 341. Breckenridge, W. H.; Kim Malmin, O.; Nikolai, W. L.; Oba, D. *Chem. Phys. Lett.* 1978, 59, 38. Breckenridge, W. H.; Kim Malmin, O. *J. Chem. Phys.* 1981, 74, 3307.
(36) Krause, L. *Adv. Chem. Phys.* 1975, 28, 267.
(37) Nikitin, E. E. *Adv. Chem. Phys.* 1975, 28, 317. Nikitin, E. E.; Smirnov, B. M. *Sov. Phys. Usp. (Engl. Transl.)* 1978, 21, 95.
(38) Hertel, I. V.; Stoll, W. *Adv. At. Mol. Phys.* 1978, 13, 113.
(39) Condon, E. U.; Shortley, G. H. *The Theory of Atomic Spectra*; Cambridge University: London, 1935. White, H. E. *Introduction to Atomic Spectra*; McGraw Hill: New York, 1934.
(40) Moore, C. E. "Atomic Energy Levels" *National Bureau of Standards Reference Data Series*; National Bureau of Standards; U.S. Government Printing Office: Washington, DC, 1971; Vol. 35.
(41) Willets, F. W. *Prog. React. Kinet.* 1971, 6, 51.
(42) Donovan, R. J.; Husain, D.; Kirsch, L. J. *Trans. Faraday Soc.* 1970, 66, 2551.
(43) Clyne, M. A. A. In *Reactive Intermediates in the Gas Phase*; Setser, D. W., Ed.; Academic: New York, 1979; p 1.
(44) Bergmann, K.; Leone, S. R.; Moore, C. B. *J. Chem. Phys.* 1975, 63, 4161.
(45) Houston, P. L. *Chem. Phys. Lett.* 1977, 47, 137.
(46) Hofmann, H.; Leone, S. R. *Chem. Phys. Lett.* 1978, 54, 314.
(47) Hofmann, H.; Leone, S. R. *J. Chem. Phys.* 1978, 69, 641.
(48) Nesbitt, D. J.; Leone, S. R. *J. Chem. Phys.* 1980, 73, 6182.
(49) Haugen, H. K.; Weitz, E.; Leone, S. R. *J. Chem. Phys.* 1985, 83, 3402. Hess, W. P.; Kohler, S. J.; Haugen, H. K.; Leone, S. R. *J. Chem. Phys.* 1986, 84, 2143.
(50) Haugen, H. K.; Weitz, E.; Leone, S. R. *Chem. Phys. Lett.* 1985, 119, 75.
(51) Gordon, E. B.; Nadkhin, A. I.; Sotnichenko, S. A.; Boriev, I. A. *Chem. Phys. Lett.* 1982, 86, 209.
(52) Boriev, I. A.; Gordon, E. B.; Efimenko, A. A. *Chem. Phys. Lett.* 1985, 120, 486.
(53) Donovan, R. J.; Husain, D. *Chem. Rev.* 1970, 70, 489.
(54) Husain, D.; Donovan, R. J. *Adv. Photochem.* 1970, 8, 1.
(55) Wiesenfeld, J. R.; Wolk, G. L. *J. Chem. Phys.* 1978, 69, 1797.
(56) Piper, L. G.; Velazco, J. E.; Setser, D. W. *J. Chem. Phys.* 1973, 59, 3323.
(57) Kolts, J. H.; Setser, D. W. *J. Chem. Phys.* 1978, 68, 4848.
(58) Felder, W.; Fontijn, A. *J. Chem. Phys.* 1978, 69, 1112.
(59) Swearengen, P. M.; Davis, S. J.; Niemczyk, T. M. *Chem. Phys. Lett.* 1978, 55, 274.
(60) Golde, M. F.; Poletti, R. A. *Chem. Phys. Lett.* 1981, 80, 23.
(61) Dreiling, T. D.; Setser, D. W. *J. Phys. Chem.* 1982, 86, 2276.
(62) Fontijn, A.; Felder, W. In *Reactive Intermediates in the Gas Phase*; Setser, D. W., Ed.; Academic: New York, 1979; p 59.
(63) Kolts, J. H.; Setser, D. W. In *Reactive Intermediates in the Gas Phase*; Setser, D. W., Ed.; Academic: New York, 1979; p 152.
(64) Kaufman, F. *J. Phys. Chem.* 1984, 88, 4909.

(65) Bergmann, K. In *Atomic and Molecular Beam Methods*; Scoles, G., Ed.; Oxford University Press: London; Vol. 1, Chapter 12, in press.
(66) Bergmann, K.; Engelhardt, R.; Hefter, U.; Witt, J. *J. Phys. E* **1979**, *12*, 507.
(67) Bergmann, K.; Hefter, U.; Witt, J. *J. Chem. Phys.* **1980**, *72*, 4777.
(68) Kroon, J. P. C.; Beijerinck, H. C. W.; Verhaar, B. J.; Verster, N. F. *Chem. Phys.* **1984**, *90*, 195.
(69) Happer, W. *Rev. Mod. Phys.* **1972**, *44*, 169.
(70) Yuh, H.-J.; Dagdigian, P. J. *J. Chem. Phys.* **1984**, *81*, 2375.
(71) Dagdigian, P. J. In *Gas-Phase Chemiluminescence and Chemi-Ionization*; Fontijn, A., Ed.; North-Holland: Amsterdam, 1985; p 203.
(72) Furio, N.; Campbell, M. L.; Dagdigian, P. J. *J. Chem. Phys.* **1986**, *84*, 4332.
(73) Campbell, M. L.; Furio, N.; Dagdigian, P. J. *Laser Chem.*, in press.
(74) Campbell, M. L.; Dagdigian, P. J. *J. Am. Chem. Soc.*, in press.
(75) Campbell, M. L.; Dagdigian, P. J. *J. Chem. Phys.*, in press.
(76) Sadeghi, N.; Setser, D. W., manuscript in preparation.
(77) Grundevik, P.; Lundberg, H.; Nilsson, L.; Olsson, G. *Z. Phys. A* **1982**, *306*, 195. Eliel, E. R.; Hogervorst, W.; Olsson, T.; Pendrill, L. R. *Z. Phys. A* **1983**, *311*, 1.
(78) Weissmann, G.; Ganz, J.; Siegel, A.; Waibel, H.; Hotop, H. *Opt. Commun.* **1984**, *49*, 335.
(79) Zare, R. N.; Dagdigian, P. J. *Science* **1974**, *185*, 739.
(80) Kinsey, J. L. *Ann. Rev. Phys. Chem.* **1977**, *28*, 349.
(81) Yuh, H.-J.; Dagdigian, P. J. *Phys. Rev. A* **1983**, *28*, 63.
(82) Majewski, W. A. *Opt. Commun.* **1983**, *45*, 201.
(83) Mestdagh, J. M.; Cuvellier, J.; Berlande, J.; Binet, A.; dePujo, P. *J. Phys. B* **1980**, *13*, 4589.
(84) Anderson, R. W.; Goddard, T. P.; Parravano, C.; Warner, J. *J. Chem. Phys.* **1976**, *64*, 4037.
(85) Apt, J.; Pritchard, D. E. *J. Phys. B* **1979**, *12*, 83.
(86) Boggy, R.; Franz, F. A. *Phys. Rev. A* **1982**, *25*, 1887.
(87) Reiland, W.; Tittes, H.-U.; Hertel, I. V. *Phys. Rev. Lett.* **1982**, *48*, 1389.
(88) Reiland, W.; Tittes, H.-U.; Hertel, I. V.; Bonacic-Koutecky, V.; Persico, M. *J. Chem. Phys.* **1982**, *77*, 1908.
(89) Düren, R.; Hasselbrink, E.; Hillrichs, G. *Chem. Phys. Lett.* **1984**, *112*, 441.
(90) Düren, R.; Hasselbrink, E.; Tischer, H. *Phys. Rev. Lett.* **1983**, *50*, 1983.
(91) van den Berg, F.; Morgenstern, R. *Chem. Phys.* **1984**, *90*, 125.
(92) Lackschewitz, U.; Maier, J.; Pauly, H. *Chem. Phys. Lett.* **1982**, *88*, 233.
(93) Jamieson, G.; Reiland, W.; Schulz, C. P.; Tittes, H.-U.; Hertel, I. V. *J. Chem. Phys.* **1984**, *81*, 5805.
(94) Cuvellier, J.; Petitjean, L.; Mestdagh, J. M.; Paillard, D.; dePujo, P.; Berlande, J. *J. Chem. Phys.* **1986**, *84*, 1451.
(95) Hüwel, L.; Maier, J.; Pauly, H. *J. Chem. Phys.* **1982**, *76*, 4961.
(96) Mestdagh, J. M.; Berlande, J.; dePujo, P.; Cuvellier, J.; Binet, A. *Z. Phys. A* **1982**, *304*, 3.
(97) Reiland, W.; Jamieson, G.; Tittes, H.-U.; Hertel, I. V. *Z. Phys. A* **1982**, *307*, 51.
(98) Bussert, W.; Bregel, T.; Allan, R. J.; Ruf, M.-W.; Hotop, H. *Z. Phys. A* **1985**, *320*, 105.
(99) Manders, M. P. I.; Driessen, J. P. J.; Beijerinck, H. C. W.; Verhaar, B. J., submitted for publication in *Phys. Rev. Lett.*
(100) Pence, W. H.; Leone, S. R. *J. Chem. Phys.* **1981**, *74*, 5707.
(101) Hale, M. O.; Leone, S. R. *J. Chem. Phys.* **1983**, *79*, 3352.
(102) Hale, M. O.; Leone, S. R. *Phys. Rev. A* **1985**, *31*, 103.
(103) Hale, M. O.; Hertel, I. V.; Leone, S. R. *Phys. Rev. Lett.* **1984**, *53*, 2296.
(104) Parson, J. M.; Ishikawa, T. *J. Chem. Phys.* **1984**, *80*, 3137.
(105) Rettner, C. T.; Zare, R. N. *J. Chem. Phys.* **1982**, *77*, 2416.
(106) Schmidt, H.; Weiss, P. S.; Mestdagh, J. M.; Covinsky, M. H.; Lee, Y. T. *Chem. Phys. Lett.* **1985**, *118*, 539.
(107) Ku, J. K.; Setser, D. W., submitted for publication in *Appl. Phys. Lett.*
(108) Böwering, N.; Bruce, M. R.; Keto, J. W. *J. Chem. Phys.* **1986**, *84*, 709, 715.
(109) Fischer, A.; Hertel, I. V. *Z. Phys. A* **1982**, *304*, 103.
(110) Schieder, R.; Walther, H.; Wöste, L. *Opt. Commun.* **1972**, *5*, 337.
(111) Düren, R.; Hoppe, H.-O.; Pauly, H. *Phys. Rev. Lett.* **1976**, *37*, 743.
(112) Bähring, A.; Hertel, I. V.; Meyer, E.; Schmidt, H. *Z. Phys. A* **1983**, *312*, 293.
(113) Bender, Ch.; Beyer, W.; Haberland, H.; Hausmann, D.; Ludescher, H.-P. *J. Phys. (Paris)* **1985**, *46*, C1–75.
(114) Nienhuis, G. *Phys. Rev. A* **1982**, *26*, 3137.
(115) Hertel, I. V.; Schmidt, H. Bähring, A.; Meyer, E. *Rep. Prog. Phys.* **1985**, *48*, 375.
(116) Lin, D.; Yu, Y. C.; Setser, D. W. *J. Chem. Phys.* **1984**, *81*, 5830.
(117) Brashears, H. C., Jr.; Setser, D. W. *J. Phys. Chem.* **1980**, *84*, 224.
(118) Kittrell, C.; Abramson, E.; Kinsey, J. L.; McDonald, S. A.; Reisner, D. E.; Field, R. W.; Katayama, D. H. *J. Chem. Phys.* **1981**, *75*, 2056.
(119) Lawrance, W. D.; Knight, A. E. W. *J. Chem. Phys.* **1982**, *76*, 5637.
(120) Reisner, D. E.; Vaccaro, P. H.; Kittrell, C.; Field, R. W.; Kinsey, J. L.; Dai, H.-L. *J. Chem. Phys.* **1982**, *77*, 573.
(121) Nebel, A.; Comes, F. J.; Stephan-Rossbach, K.-H. *Chem. Phys.* **1985**, *94*, 257.
(122) Golde, M. F.; Poletti, R. A. *Chem. Phys. Lett.* **1981**, *80*, 18.
(123) Golde, M. F.; Ho, Y.-S. *J. Chem. Phys.* **1985**, *82*, 3160.
(124) Pitre, J.; Hammond, K.; Krause, L. *Phys. Rev. A* **1972**, *6*, 2101.
(125) Horiguchi, H.; Tsuchiya, S. *Bull. Chem. Soc. Jpn.* **1971**, *44*, 1213.
(126) Haberman, J. A.; Wilcomb, B. E.; van Itallie, F. J.; Bernstein, R. B. *J. Chem. Phys.* **1975**, *62*, 4466; erratum, **1975**, *63*, 2772.
(127) Hayashi, S.; Mayer, T. M.; Bernstein, R. B. *Chem. Phys. Lett.* **1978**, *53*, 419.
(128) Liu, K.; Parson, J. M. *J. Chem. Phys.* **1976**, *65*, 815.
(129) Krause, H. F.; Johnson, S. G.; Datz, S.; Schmidt-Bleek, F. K. *Chem. Phys. Lett.* **1975**, *31*, 577.
(130) Krause, H. F.; Datz, S.; Johnson, S. G. *J. Chem. Phys.* **1973**, *58*, 367.
(131) Hepburn, J. W.; Liu, K.; Macdonald, R. G.; Northrup, F. J.; Polanyi, J. C. *J. Chem. Phys.* **1981**, *75*, 3353.
(132) Ramsey, N. F. *Molecular Beams*; Clarendon Press: Oxford, 1956.
(133) Gersh, M. E.; Muschlitz, E. E. *J. Chem. Phys.* **1973**, *59*, 3538.
(134) Baer, T. In *Gas Phase Ion Chemistry*; Bowers, M. T., Ed.; Academic: New York, 1979; Vol. 1, p 153.
(135) Sampson, J. A. R.; Cairns, R. B. *Phys. Rev.* **1968**, *173*, 80.
(136) Rakshit, A. B.; Warneck, P. *J. Chem. Phys.* **1980**, *73*, 2673.
(137) Lindinger, W.; Howorka, F.; Futrell, J. H.; Dotan, I. *J. Chem. Phys.* **1981**, *74*, 4750. See, however: Rakshit, A. B.; Warneck, P. *J. Chem. Phys.* **1981**, *74*, 4751.
(138) Beadle, P.; Dunn, M. R.; Jonathan, N. B. H.; Liddy, J. P.; Naylor, J. C. *J. Chem. Soc., Faraday Trans. 2* **1978**, *74*, 2170.
(139) Maylotte, D. H.; Polanyi, J. C.; Woodall, K. B. *J. Chem. Phys.* **1972**, *57*, 1547.
(140) Polanyi, J. C.; Skrlac, W. J. *Chem. Phys.* **1977**, *23*, 167.
(141) Brandt, D.; Dickson, L. W.; Kwan, L. N. Y.; Polanyi, J. C. *Chem. Phys.* **1979**, *39*, 189.
(142) Sung, J. P.; Setser, D. W. *Chem. Phys. Lett.* **1977**, *48*, 413.
(143) Tamagake, K.; Setser, D. W.; Sung, J. P. *J. Chem. Phys.* **1980**, *73*, 2203.
(144) Agrawalla, B. S.; Singh, J. P.; Setser, D. W. *J. Chem. Phys.* **1983**, *79*, 6416.
(145) Brunet, H.; Chauvet, Ph.; Mabru, M.; Torchin, L. *Chem. Phys. Lett.* **1985**, *117*, 371.
(146) Engleman, R.; Palmer, B. A.; Davis, S. J. *J. Opt. Soc. Am.* **1983**, *73*, 1585.
(147) Husain, D.; Slater, N. K. H.; Wiesenfeld, J. R. *Chem. Phys. Lett.* **1979**, *51*, 201.
(148) Garstang, R. H. *J. Res. Natl. Bur. Stand. Sect. A* **1964**, *68*, 61.
(149) Wiesenfeld, J. R.; Wolk, G. L. *J. Chem. Phys.* **1978**, *69*, 1805.
(150) Burak, I.; Eyal, M. *Chem. Phys. Lett.* **1977**, *52*, 534.
(151) Hepburn, J. W. *Isr. J. Chem.* **1984**, *24*, 273.
(152) Bokor, J.; Freeman, R. R.; White, J. C.; Storz, R. H. *Phys. Rev. A* **1981**, *24*, 612.
(153) Bischel, W. K.; Perry, B. E.; Crosley, D. R. *Chem. Phys. Lett.* **1981**, *82*, 85.
(154) Heaven, M.; Miller, T. A.; Freeman, R. R.; White, J. C.; Bokor, J. *Chem. Phys. Lett.* **1982**, *86*, 458.
(155) Brewer, P.; van Veen, N.; Bersohn, R. *Chem. Phys. Lett.* **1982**, *91*, 126.
(156) Das, P.; Ondrey, G.; van Veen, N.; Bersohn, R. *J. Chem. Phys.* **1983**, *79*, 724.
(157) Brewer, P.; Das, P.; Ondrey, G.; Bersohn, R. *J. Chem. Phys.* **1983**, *79*, 720.
(158) Tiee, J. J.; Ferris, M. J.; Loge, G. W.; Wampler, F. B. *Chem. Phys. Lett.* **1983**, *96*, 422.
(159) Das, P.; Venkitachalam, T.; Bersohn, R. *J. Chem. Phys.* **1984**, *80*, 4859.
(160) Venkitachalam, T. V.; Das, P.; Bersohn, R. *J. Am. Chem. Soc.* **1983**, *105*, 7452.
(161) Herzberg, G., *Molecular Spectra and Molecular Structure. I. Spectra of Diatomic Molecules*; D. Van Nostrand: Princeton, 1950.
(162) Tully, J. C. *J. Chem. Phys.* **1974**, *60*, 3042.
(163) Komornicki, A.; Morokuma, K.; George, T. F. *J. Chem. Phys.* **1977**, *67*, 5012.
(164) Last, I.; Baer, M. *J. Chem. Phys.* **1985**, *82*, 4954.
(165) Rebentrost, F.; Lester, W. A., Jr. *J. Chem. Phys.* **1975**, *63*, 3737; **1976**, *64*, 3879, 4223; **1977**, *67*, 3367.

(166) Wyatt, R. E.; Walker, R. B. *J. Chem. Phys.* **1979**, *70*, 1501.
(167) Neumark, D. M.; Wodtke, A. M.; Robinson, G. N.; Hayden, C. C.; Lee, Y. T. *J. Chem. Phys.* **1985**, *82*, 3045.
(168) Clyne, M. A. A.; Cruse, H. W. *J. Chem. Soc., Faraday Trans. 2* **1972**, *68*, 1377.
(169) Donovan, R. J.; Hathorn, F. G. M.; Husain, D. *Trans. Faraday Soc.* **1968**, *64*, 1228.
(170) Deakin, J. J.; Husain, D. *J. Photochem.* **1972/73**, *1*, 353.
(171) Hall, G. E.; Arepalli, S.; Houston, P. L.; Wiesenfeld, J. R. *J. Chem. Phys.* **1985**, *82*, 2590.
(172) Lilenfeld, H. V.; Whitefield, P. D.; Bradburn, G. R. *J. Phys. Chem.* **1984**, *88*, 6158.
(173) Clyne, M. A. A.; Nip, W. S. *Int. J. Chem. Kinet.* **1977**, *10*, 365.
(174) Cadman, P.; Polanyi, J. C. *J. Phys. Chem.* **1968**, *72*, 3715.
(175) Anlauf, K. G.; Horne, D. S.; Macdonald, R. G.; Polanyi, J. C.; Woodall, K. B. *J. Chem. Phys.* **1972**, *57*, 1561.
(176) Sung, J. P.; Malins, R. J.; Setser, D. W. *J. Phys. Chem.* **1979**, *83*, 1007.
(177) Dinur, U.; Kosloff, R.; Levine, R. D.; Berry, M. J. *Chem. Phys. Lett.* **1975**, *34*, 199.
(178) Trickl, T.; Wanner, J. *J. Chem. Phys.* **1983**, *78*, 6091.
(179) Fletcher, I. W.; Whitehead, J. C. *J. Chem. Soc., Faraday Trans. 2* **1982**, *78*, 1165.
(180) Fotakis, C.; Donovan, R. J. *J. Chem. Soc., Faraday Trans. 2* **1979**, *75*, 1553.
(181) Spencer, D. J.; Wittig, C. *Opt. Lett.* **1979**, *4*, 1.
(182) Stedman, D. H.; Setser, D. W. *Prog. React. Kinet.* **1971**, *6*, 193.
(183) Golde, M. F. In *Gas Kinetics and Energy Transfer, Specialist Periodical Reports*; Ashmore, P. G., Donovan, R. J., Eds.; Chemical Society: London, 1976; Vol. 2, p 121.
(184) Rhodes, C. K., Ed. *Excimer Lasers*; Springer-Verlag: Berlin, 1979.
(185) Piper, L. G.; Setser, D. W.; Clyne, M. A. A. *J. Chem. Phys.* **1975**, *63*, 5018.
(186) Gundel, L. A.; Setser, D. W.; Clyne, M. A. A.; Coxon, J. A.; Nip, W. S. *J. Chem. Phys.* **1976**, *64*, 4390.
(187) Setser, D. W.; Dreiling, T. D.; Brashears, H. C., Jr.; Kolts, J. H. *Faraday Discuss. Chem. Soc.* **1979**, *67*, 255.
(188) Dunning, T. H., Jr.; Hay, P. J. *J. Chem. Phys.* **1978**, *69*, 134. Hay, P. J.; Dunning, T. H., Jr. *J. Chem. Phys.* **1978**, *69*, 2209.
(189) Johnson, K.; Simons, J. P.; Smith, P. A.; Washington, C.; Kvaran, A. *Mol. Phys.* **1986**, *57*, 255.
(190) Chambaud, G.; Lévy, B.; Pernot, P. *Chem. Phys.* **1985**, *95*, 299.
(191) Hartman, D. C.; Winn, J. S. *J. Chem. Phys.* **1981**, *74*, 4320.
(192) Chupka, W. A.; Russell, M. E. *J. Chem. Phys.* **1968**, *49*, 5426.
(193) Kuntz, P. J.; Roach, A. C. *J. Chem. Soc., Faraday Trans. 2* **1972**, *68*, 259.
(194) Chapman, S.; Preston, R. K. *J. Chem. Phys.* **1974**, *60*, 650.
(195) Ng, C. Y., private communication.
(196) Spalburg, M. R.; Gislason, E. A. *Chem. Phys.* **1985**, *94*, 339.
(197) Govers, T. R.; Guyon, P. M.; Baer, T.; Cole, K.; Fröhlich, H.; Lavollée, M. *Chem. Phys.* **1984**, *87*, 373.
(198) Johnson, R. E. *J. Phys. Soc. Jpn.* **1972**, *32*, 1612.
(199) Dagdigian, P. J. *Chem. Phys. Lett.* **1978**, *55*, 239.
(200) Telle, H.; Brinkmann, U. *Mol. Phys.* **1980**, *39*, 361.
(201) Gislason, E. A. In *Alkali Halide Vapors*; Davidovits, P.; McFadden, D. L., Eds.; Academic: New York, 1979; p 415.
(202) Honjou, N.; Yarkony, D. R. *J. Phys. Chem.* **1985**, *89*, 2919, and unpublished results.
(203) Menzinger, M. In "Gas-Phase Chemiluminescence and Chemi-Ionization"; Fontijn, A., Ed.; North-Holland: Amsterdam, 1985; p 25.
(204) Alexander, M. H.; Orlikowski, T.; Straub, J. E. *Phys. Rev. A* **1983**, *28*, 73. Pouilly, B.; Orlikowski, T.; Alexander, M. H. *J.*

(205) *Phys. B* **1985**, *18*, 1953.
Alexander, M. H. In "Gas-Phase Chemiluminescence and Chemi-Ionization"; Fontijn, A., Ed.; North-Holland: Amsterdam, 1985; p 221.
(206) Wodarczyk, F. J.; Harker, A. B. *Chem. Phys. Lett.* **1979**, *62*, 529.
(207) Tang, K. Y.; Hunter, R. O., Jr.; Oldenettel, J.; Huestis, D. L. *J. Chem. Phys.* **1979**, *70*, 1492.
(208) Dreiling, T. D.; Setser, D. W. *J. Chem. Phys.* **1983**, *79*, 5423, 5439.
(209) Helvajian, H.; Wittig, C. *J. Chem. Phys.* **1982**, *76*, 3505.
(210) Callear, A. B.; McGurk, J. C. *J. Chem. Soc., Faraday Trans. 2* **1972**, *68*, 289.
(211) Huber, K. P.; Herzberg, G. *Molecular Spectra and Molecular Structure. IV. Constants of Diatomic Molecules*; Van Nostrand Reinhold: New York, 1979.
(212) Chowdhury, M. A.; Husain, D. *J. Photochem.* **1977**, *7*, 41.
(213) Wiesenfeld, J. R.; Yuen, M. J. *J. Phys. Chem.* **1978**, *82*, 1225.
(214) Chowdhury, M. A.; Husain, D. *J. Photochem.* **1979**, *10*, 277.
(215) Brown, A.; Husain, D. *Can. J. Chem.* **1976**, *54*, 4.
(216) Wiesenfeld, J. R.; Yuen, M. J. *Chem. Phys. Lett.* **1976**, *42*, 293.
(217) Chowdhury, M. A.; Husain, D. *J. Chem. Soc., Faraday Trans. 2* **1978**, *74*, 1065.
(218) Linevsky, M. J.; Carabetta, R. A. *Chemical Laser Potential of Selected Group IVA Metal Oxides*; Kirtland AFB, NM, 1976; AFWL-TR-77-121.
(219) Foo, P. D.; Wiesenfeld, J. R.; Husain, D. *Chem. Phys. Lett.* **1975**, *32*, 443.
(220) Husain, D.; Littler, J. G. F. *J. Photochem.* **1973**, *2*, 247.
(221) Husain, D.; Littler, J. G. F. *Int. J. Chem. Kinet.* **1974**, *6*, 61.
(222) Ewing, J. J.; Trainor, D. W.; Yatsiv, S. *J. Chem. Phys.* **1974**, *61*, 4433.
(223) Husain, D.; Young, A. N. *J. Chem. Soc., Faraday Trans. 2* **1975**, *71*, 525.
(224) Husain, D.; Norris, P. E. *J. Chem. Soc., Faraday Trans. 2* **1978**, *74*, 93.
(225) Harding, D. R.; Husain, D. *J. Chem. Soc., Faraday Trans. 2* **1984**, *80*, 615.
(226) Brown, A.; Husain, D. *J. Chem. Soc., Faraday Trans. 2* **1975**, *71*, 699.
(227) Foo, P. D.; Wiesenfeld, J. R.; Yuen, M. J.; Husain, D. *J. Phys. Chem.* **1976**, *80*, 91.
(228) Husain, D.; Littler, J. G. F. *Combust. Flame* **1974**, *22*, 295.
(229) Bevan, M. J.; Husain, D. *J. Photochem.* **1975**, *4*, 51.
(230) Bevan, M. J.; Husain, D. *J. Phys. Chem.* **1976**, *80*, 217.
(231) Bevan, M. J.; Husain, D. *J. Photochem.* **1974/5**, *3*, 1.
(232) Donovan, R. J.; Husain, D. *Annu. Rep. Prog. Chem., Sect. A: Gen. Phys. Inorg. Chem.* **1972**, *68*, 124. Donovan, R. J.; Husain, D.; Kirsch, L. J. *Annu. Rep. Prog. Chem., Sect. A: Gen., Phys. Inorg. Chem.* **1973**, *69*, 19.
(233) Gedeon, A.; Edelstein, S. A.; Davidovits, P. *J. Chem. Phys.* **1971**, *55*, 5171.
(234) Bellisio, J. A.; Davidovits, P. *J. Chem. Phys.* **1970**, *53*, 3474.
(235) Wiesenfeld, J. R. *Chem. Phys. Lett.* **1973**, *21*, 517.
(236) In this paper the periodic group notation in parentheses is in accord with recent actions by IUPAC and ACS nomenclature committees. A and B notation is eliminated because of wide confusion. Groups IA and IIA become groups 1 and 2. The d-transition elements comprise groups 3 through 12, and the p-block elements comprise groups 13 through 18. (Note that the former Roman number designation is preserved in the last digit of the numbering: e.g., III → 3 and 13.)
(237) Weiser, C.; Siska, P. E. *J. Chem. Phys.*, in press.
(238) Zhang, F. M.; Oba, D.; Setser, D. W., to be submitted for publication.